Palaeogeography, Palaeoclimatology, Palaeoecology 682 (2026) 113421

Contents lists available at ScienceDirect

Palaeogeography, Palaeoclimatology, Palaeoecology

journal homepage: www.elsevier.com/locate/palaeo

Revisiting the age of the Fish Canyon sanidine dating standard☆

Klaudia F. Kuiper [a], Zoë Toorenburgh [b], Jörn-Frederik Wotzlaw [b], Christian Zeeden [c], Francisco J. Sierro [d], Joshua H.F.L. Davies [e], Diana Sahy [f], Daniel J. Condon [f], Frederik J. Hilgen [g,*]

[a] Department of Earth Sciences, Faculty of Science, Vrije Universiteit, De Boelelaan 1085, 1081 HV Amsterdam, the Netherlands
[b] Institute of Geochemistry and Petrology, Department of Earth Sciences, ETH Zurich, Zurich CH-8092, Switzerland
[c] LIAG Institute for Applied Geophysics, Stilleweg 2, 30655 Hannover, Germany
[d] Department of Geology, University of Salamanca, Plaza de la Merced s/n, 37008 Salamanca, Spain
[e] Département des Sciences de la Terre et de l'Atmosphère/Geotop, Université du Québec à Montréal, Montréal H3C 3P8, QC, Canada
[f] British Geological Survey, Keyworth, NG12 5GG Nottingham, UK
[g] Department of Earth Sciences, Utrecht University, Princetonlaan 8a, 3584 CB Utrecht, the Netherlands

ARTICLE INFO

Editor: L Angiolini

Keywords:
Fish Canyon sanidine
Fish Canyon Tuff
Ar/Ar dating
U/Pb dating
Astronomical dating
Geological time scale

ABSTRACT

In 2008, Kuiper and others published an astronomically calibrated age of 28.201 ± 0.046 Ma for the Fish Canyon sanidine (FCs), the most widely used standard in Ar/Ar dating. This age was incorporated in GTS2012 and GTS2020, but has been challenged by later studies that used various approaches, leading again to a ~ 1.5 % age scattering. This uncertainty hampers the construction of a uniform and coherent time scale that is key to modern high-resolution, multi-disciplinary studies in Earth history. To solve this ongoing uncertainty, we present 1) a visual and statistical re-examination of the astronomical tuning on which the FCs age of 28.201 Ma is based and 2) new single crystal U/Pb ID-TIMS zircon ages of the astronomically calibrated Faneromeni A1 ash bed and the Fish Canyon Tuff (FCT).

Our results corroborate the initial tuning and invalidate astronomical and U/Pb based FCs age calibrations, which are much younger or older. The preferred astronomical calibration seems to converge to a slightly younger age of 28.171–28.176 Ma. This is in good agreement with our new Bayesian zircon eruption age of 28.171 + 0.039/− 0.044 Ma for the FCT and the recently published Bayesian calibration of the 40 K decay scheme with a coupled FCs age of 28.183 ± 0.070 Ma. Importantly, the astronomical and U/Pb-based calibrations now yield similar ages, implying mutual agreement between the three main dating methods to construct our time scale. However, by contrast, the Cretaceous/Paleogene (K/Pg) boundary, which represents a critical triple point for the intercalibration, now produces divergent ages.

In summary, much progress has been made in solving the critical issue of the age of the FCs dating standard. For the moment, we either recommend the continued use of the astronomically calibrated age of 28.201 ± 0.046 Ma or, preferentially, a slightly younger age of 28.171–28.176 Ma. We further endorse investigation in a community-based effort where new data and improved methodologies may lead to further insight into fundamental properties and potentially a definitive age not only for the FCs dating standard, but importantly also for the K/Pg boundary.

1. Introduction

Sanidine of the Fish Canyon tuff (FCs) represents the most widely used standard in $^{40}Ar/^{39}Ar$ dating. However, ongoing debate about its age results in substantial uncertainties in $^{40}Ar/^{39}Ar$ ages, hampering 1) detailed comparison with $^{40}Ar/^{39}Ar$ ages using different standards and/or standard ages and with other dating methods, and 2) the incorporation of $^{40}Ar/^{39}Ar$ ages in the geological time scale. In the late nineties and 2000's, $^{40}Ar/^{39}Ar$ data were commonly reported relative to FCs of 28.02 Ma (Renne et al., 1998). This age is based on intercalibration with

☆ This article is part of a Special issue entitled: 'From rock to time' published in Palaeogeography, Palaeoclimatology, Palaeoecology.

* Corresponding author.
E-mail address: f.j.hilgen@uu.nl (F.J. Hilgen).

https://doi.org/10.1016/j.palaeo.2025.113421
Received 1 May 2025; Received in revised form 27 October 2025; Accepted 11 November 2025
Available online 14 November 2025

the primary biotite standard GA1550 and has a full external uncertainty (including decay constants uncertainty based on Steiger and Jäger (1977) of ~1 % (± 0.28 Ma). Because intrinsic uncertainties in $^{40}Ar/^{39}Ar$ dating were likely even larger, in the order of 2–2.5 % (Min et al., 2000), recent ages for the FCs were derived from intercalibration with alternative, astronomical and U/Pb, dating methods and model optimization approaches instead of intercalibration relative to a primary K-Ar dated standard.

The study of Kuiper et al. (2008) provided an important next step in the astronomical calibration of the FCs, building upon earlier studies that either compared $^{40}Ar/^{39}Ar$ and astronomical age estimates of Quaternary magnetic reversals (e.g., Baksi et al., 1992; McDougall et al., 1992; Spell and McDougall, 1992; Tauxe et al., 1992; Renne et al., 1994) or used less suitable minerals such as plagioclase or biotite (Hilgen et al., 1997; Kuiper et al., 2004) for $^{40}Ar/^{39}Ar$ dating of volcanic ash layers in astronomically dated successions for this purpose. The FCs age of 28.201 ± 0.046 Ma (2σ, incl. analytical, decay constant and astronomical age uncertainties) of Kuiper et al. (2008) is based on a direct comparison of astronomical and single crystal $^{40}Ar/^{39}Ar$ sanidine ages of volcanic ash layers in tuned marine sections of late Miocene (Messinian) age in the Mediterranean. The ash layers are intercalated in marine sections in Morocco; these sections are correlated cyclostratigraphically to tuned sections elsewhere in the Mediterranean by means of high-resolution planktonic foraminifera biostratigraphy to obtain astronomical ages for the ash layers and an astronomically calibrated age for the FCs through a detailed comparison with single crystal $^{40}Ar/^{39}Ar$ sanidine ages for the same ash layers.

This FCs age of 28.201 ± 0.046 Ma has subsequently been confirmed by several studies (e.g., Rivera et al., 2011: 28.172 ± 0.028 Ma; Wotzlaw et al., 2013; 28.196 ± 0.038 Ma; Phillips et al., 2022: 28.176 ± 0.023 Ma), and has been adopted in the standard Geological Time Scale (GTS2012/2020: Gradstein et al., 2012, 2020), but has also been seriously challenged by alternative – much – younger astronomical FCs ages of 27.89 Ma (Westerhold et al., 2012), 27.93 Ma (Channell et al., 2010), 28.083 ± 0.045 Ma (Drury et al., 2017) and 28.10 Ma (Westerhold et al., 2015) as well as older U/Pb based ages of 28.294 ± 0.072 Ma (2σ, age uncertainty based on Monte Carlo simulation) (Renne et al., 2010, 2011), using statistical optimization and ^{40}K activity data, K/Ar isotopic data, and selected $^{238}U/^{206}Pb$ – $^{40}Ar/^{39}Ar$ data pairs as input, and 28.393 ± 0.194 Ma (Ganerød et al., 2011) (see also Table 1). Recently, a novel Bayesian calibration of the 40 K decay scheme was published using U/Pb dating to arrive at an FCs age of 28.183 ± 0.070 Ma (2σ, incl. R-value, decay constant and neutron fluence monitor uncertainties) (Carter et al., 2025). This modeling also produced age calibrated decay constants.

All methods and approaches received both support and criticism during the last 17 years. The present paper is intended to test the different astronomical and U/Pb based calibrations by presenting relevant new data. It does not follow the structure of a regular paper as it combines these new data with a review of the cyclostratigraphy of the Mediterranean late Miocene. We will start with this in depth review followed by a statistical evaluation of the astronomical calibration of the deep marine sections in the Mediterranean on which the currently widely used FCs age of 28.201 Ma is based. This is done by using a new quantitative proxy time series between 6.8 and 6.0 Ma to test various tunings that are consistent with different FCs ages. We will continue with introducing new U/Pb ages of the Faneromeni A1 ash bed and the FCT that are relevant for independently determining the FCs age. This is succeeded by a discussion in which we look at the consequences of our relevant new data with the various ages that have been published for the FCs standard over the years. At the end, recommendations are made for the age of the FCs to be used in the coming years (including the next revision of the standard GTS), including a forward look on methodological developments in $^{40}Ar/^{39}Ar$ geochronology. Finally, a community-based effort directed at new data and improved methodologies may lead to better insight into fundamental properties and potentially a slightly different age of the standard. This effort will help clarifying whether alternative approaches to the astronomical calibration, such as statistical optimization, Bayesian modeling or direct U/Pb FCT zircon dating, produce an even more accurate and precise FCs age. Age uncertainties, if available are reported the first time an age is mentioned in the text. They are reported at 2σ full uncertainty, including both internal and external errors as specified in the original publications, unless stated otherwise.

2. Review and statistical evaluation of the astronomical tuning of the Mediterranean Miocene

We will first review and statistically evaluate the astronomical age model for Miocene sections in the Mediterranean on which the astronomically calibrated age of 28.201 ± 0.046 Ma of Kuiper et al., 2008) is based. The tuning of marine Miocene land-based sections in the Mediterranean (e.g., Hilgen and Krijgsman, 1999; Hilgen et al., 1995; Krijgsman et al., 1997; Sierro et al., 2001; Van Assen et al., 2006; see Fig. 1 for location) partially underlies the age calibration of the late Miocene portion of the standard GTS2012/2020 (Hilgen et al., 2012; Raffi et al., 2020) and the astronomical calibration of the FCs (Kuiper et al., 2008; Rivera et al., 2011), used in GTS2012 (Schmitz, 2012) and more recently in GTS2020 (Schmitz et al., 2020). It is important to realize that the Pleistocene and Eocene calibrations of Channell et al. (2010) and Westerhold et al. (2012) (see paragraph 2.c), which are linked to astronomically calibrated FCs ages of 27.93 and 27.89 Ma, respectively, imply that the Miocene tuning of the Mediterranean is too old by ~70 kyr, or ~ 3 precession cycles, while the optimization

Table 1
Overview of recent FCs and FCT ages based on different methods and approaches. Ages refer to a) Renne et al. (1998); b) Westerhold et al. (2012); c) Channell et al. (2010); d) Drury et al. (2017); f) Channell et al. (2020); g) Rivera et al. (2011); h) Phillips et al. (2022); i) Kuiper et al. (2008); j) this paper; k) Keller et al. (2018); m) Wotzlaw et al. (2013); and n) Renne et al. (2011); and o) Ganerød et al. (2011).

FCs age	Ar/Ar		Astronomical		U/Pb	
	Age	Calibration	Age	Method/solution	Age	
Youngest	**28.02 ± 0.28**[a]	GA-1550 biotite	**27.89**[b]	Brunhes-Matuyama		
			27.93[c]			
Younger			**28.083 ± 0.045**[d]			
			28.10[e]			
			28.15[f]	magnetic reversals	**28.171 + 0.039/− 0.044**[j]	eruption age
			28.172 ± 0.028[g]	La2004	**28.186 ± 0.037**[k]	eruption age
			28.176 ± 0.023[h]	La2004		
					28.183 ± 0.070[l]	Bayesian
Young ages			**28.201 ± 0.046**[i]	La2004	**28.196 ± 0.038**[m]	youngest grain
					28.194 ± 0.034[j]	youngest population
Older					**28.294 ± 0.072**[n]	optimization
					28.393 ± 0.194[o]	paired Ar/Ar-U/Pb

Fig. 1. Location map of Mediterranean sections. The location of Oued Akrech on the Atlantic side of Morocco, and the Casanieves borehole and Zumaia section on the Atlantic side of Spain are also shown. Google maps coordinates for most of the important sections in alphabetical order: Aghios Ioannis: 35.067889°, 24.906194° (latitude, longitude); Falconara: 37.128952°, 14.021020°; Faneromeni: 35.223642°, 26.063496°; Kastelli: 35.076611°, 24.925194°; Messadit: 35.351252°, −3.024708°; Metochia A/B: 34.855518°, 24.089234°; Metochia D: 34.858349°, 24.092606°; Monte del Casino: 44.261130°, 11.628464°; and Oued Akrech: 33.925104°, −6.809047°. Sections of the Abad marl composite section in Spain (see Sierro et al., 2001): Gafares: 37.025503°, −1.978324°; Gypsum Quarry A: 37.073751°, −2.087092°; Gypsum Quarry B: 37.077288°, −2.090587°; Molinas A: 37.090183°, −2.069826°; Molinas B: 37.091238°, −2.070402°; and Perales C: 37.097268°, −2.055176.

approach yielding 28.294 Ma (Renne et al., 2010, 2011) implies a tuning that is one cycle too young. Below we re-evaluate the original tuning for the critical interval between 7.6 and 6.0 Ma and delineate cycle patterns on which it is based in detail. We will then use a new quantitative proxy record to statistically evaluate both this tuning as well as other tuning options that are consistent with the alternative astronomical and U/Pb based FCs calibrations.

2.1. Review of astronomical age model for the Mediterranean Miocene

2.1.1. 7.6–6.8 Ma

From 7.6 to 6.8 Ma, the Mediterranean record contains two large-scale sapropel clusters tuned to 405-kyr eccentricity maxima at 7.45 and 7.05 Ma (blue stars VII and VIII in Fig. 2; Hilgen et al., 1995). Cluster VII is atypical as it coincides with a 2.4 Myr eccentricity minimum, resulting in relatively low and constant precession amplitudes, a poorly developed ~100-kyr cyclicity and a relatively strong influence of obliquity. The tuning of the sapropel and carbonate cycles in this cluster is therefore constrained by precession-obliquity interference patterns (M69–71, G83–86, K9–13, F2–6, C15–17 and OA1–18 in Fig. 2; see also Hilgen et al., 1995, 2000; Krijgsman et al., 1997). Moreover, the total number of cycles in the Faneromeni (Crete, Greece) and Oued Akrech (Atlantic side of Morocco) sections in which all cycles are lithologically expressed, is identical (e.g., F7–18 and OA7–18 in Fig. 2).

Cluster VIII starts with a very prominent basal sapropel that is recognized in all sections in the Mediterranean and, as a thick and distinct reddish layer, at Oued Akrech (M74, K14, F18, C18, OA18; Fig. 2). This sapropel overlies a thick marly interval in which sapropels are either absent or very rare and thin as in section Metochia; this marly interval marks the 405-kyr minimum around 7.25 Ma. The two thin sapropels (M72–73) that are present in this interval correspond to the strongest summer insolation maxima and coincide with the First Occurrence (FO) of *Globorotalia menardii* 5 and the First Regular Occurrence (FRO) of the *Globorotalia miotumida* group in the Mediterranean, respectively. They correlate with the two thickest and most distinct reddish layers in this interval at Oued Akrech (OA9 and 15). These reddish layers coincide with the same planktonic foraminiferal events as the correlative thin sapropels in the Metochia section (Hilgen et al., 2000).

The first prominent sapropel of cluster VIII marks the beginning of a characteristic pattern related to precession-obliquity interference recognized in all sections (e.g., M74–78; K14–17; F18–22; C18–22; OA18–20) and in the astronomical target curve (Fig. 2). Other details that can easily be identified both in the target curve and in the geological record are 1) the weakly developed sapropel or correlative grey layer (F26, C26, M85) that corresponds to the weakest insolation maximum at 7.10 Ma and 2) the anomalously thick cycle dated astronomically at 6.9 Ma (F29, C29) (Fig. 2). The latter marks a double precession cycle in which the younger one is not developed as a consequence of the very weak Insolation forcing. The sapropel pattern of cluster VIII is succeeded by two thin sapropels of which the younger coincides with the *Globorotalia nicolae* First Occurrence (FO) and may be developed as grey marl or not at all (F33, M91–92, C33). Together they mark the ~100- and 405-kyr eccentricity minimum at 6.82 Ma.

2.1.2. 6.8–6.25 Ma

Tuning the interval younger than 6.8 Ma is less straightforward, due to stratigraphic complications in some of the sections (e.g. slump levels, shearplanes) and the more complex cycle buildup with diatomites in addition to sapropels and homogeneous marls (Fig. 3). On the other hand, the geophysical well logs of the Casanieves borehole located just outside the Mediterranean (Ledesma, 2000) reveal an excellent fit with

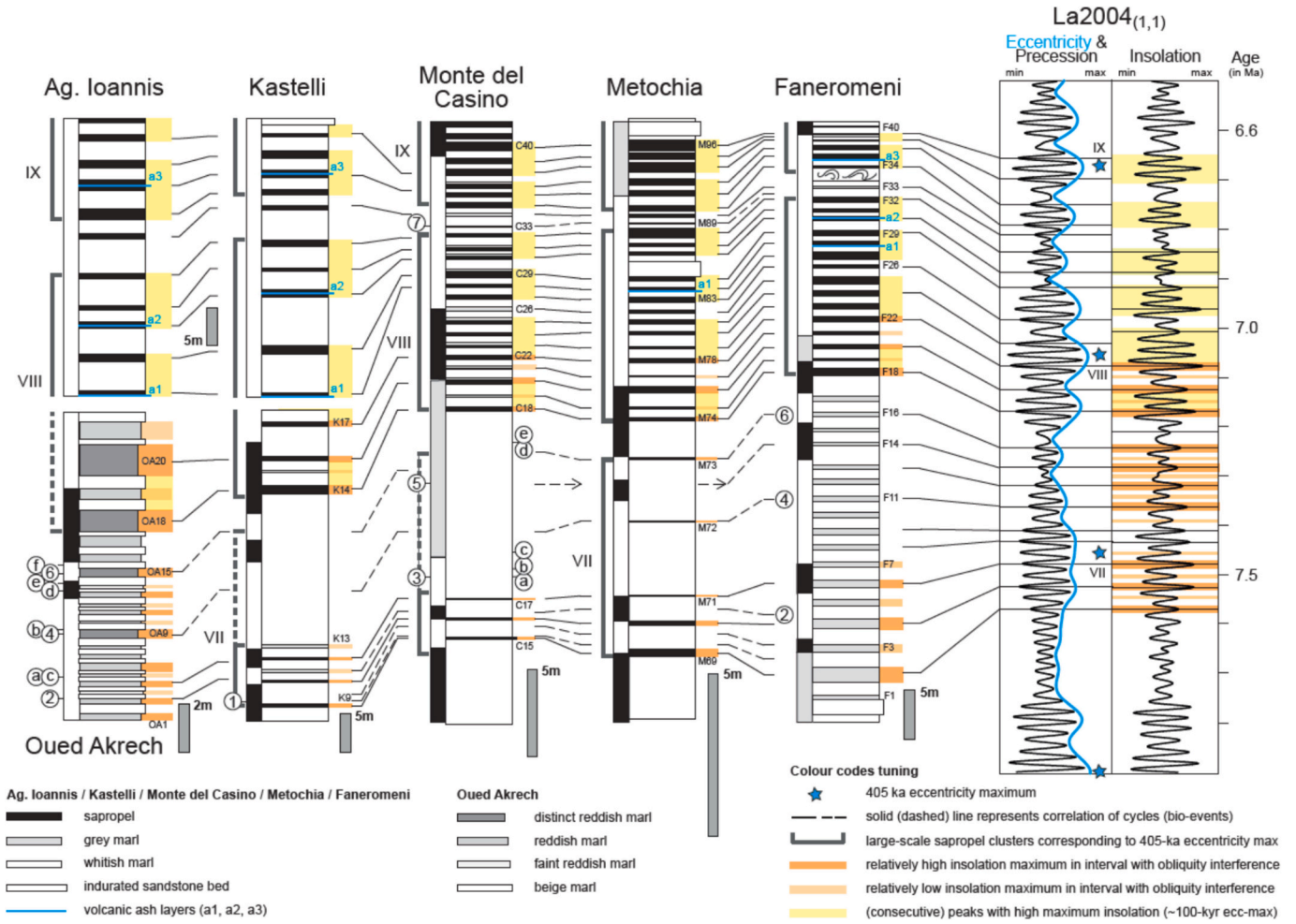

Fig. 2. Integrated magnetobiocyclostratigraphic correlations between selected Mediterranean sections and the Oued Akrech section in Morocco, and astronomical tuning of these sections for the interval between 7.6 and 6.8 Ma. Labeled calcareous plankton bio-events: 1) d/s coiling change *Globorotalia scitula* Group, 2) Last Common Occurrence (LCO) *Globorotalia menardii* 4, 3) Last Occurrence (LO) *Globorotaloides falconarae*, 4) Last Occurrence *Globorotalia menardii* 5, 5) Last Occurrence (LO) *G, menardii* 4, 6) First Regular Occurrence (FRO) *Globorotalia miotumida* Group, 7) First occurrence (FO) *Globorotalia nicolae*, and a) First Occurrence (FO) *Amaurolithus primus*, b) First Occurrence (FO) *Reticulofenestra rotaria*, c) First Occurrence (FO) *Amaurolithus* aff. *amplificus*, d) First Occurrence (FCO) *R. rotaria*, e) First Occurrence (FO) *Amaurolithus delicatus*, and f) First Common Occurrence (FCO) *A. delicatus*. Sapropels and related grey (Faneromeni) and reddish (Oued Akrech) marls have been labeled per section. In addition, the position of ash layers a1–3 has been indicated.

boreal summer insolation, especially as far as eccentricity related variations in precession amplitude are concerned (Fig. 3). The Casanieves record can be linked to the Mediterranean sections by means of planktonic foraminiferal biostratigraphy and confirm our tuning (Fig. 3). Besides, cycles UA1–8 of the Upper Abad (Sorbas, Spain) comprise a group of distinct sapropels, which together mark all the precession cycles associated with the two youngest ~100-kyr cycles in the 405-kyr eccentricity maximum around 6.67 Ma, while the three faintly laminated marls of cycles LA17–19 in the older sections of the Lower Abad denote the oldest ~100-kyr maximum with an age of 6.77 Ma at the beginning of this 405-kyr maximum (Fig. 3; note, that a 405-kyr eccentricity cycle usually comprise 4x100-kyr cycles of which 2 or 3 have a more pronounced amplitude during a 405-kyr eccentricity maximum; note further the presence of the complex multiple slump level between the Lower and Upper Abad in the Sorbas basin, see Sierro et al., 2001). The interval with less distinct sapropels (UA9–13, except for UA8) marks the next younger 405-kyr minimum around 6.5 Ma (I in Fig. 3). This is followed by two clusters of three rather well defined sapropels (UA14–16 and 18–20) with one weaker developed sapropel in between (of UA17). These two clusters mark the first two ~100-kyr eccentricity maxima following the 405-kyr minimum at 6.5 Ma. The weaker developed sapropel of UA17 with the thick homogeneous and/or diatomaceous interval on top corresponds to the ~100-kyr eccentricity minimum around 6.36 Ma (Fig. 3). The main sinistral to dextral coiling change in neogloboquadrinids is associated with this minimum (Sierro et al., 2001).

However, the most distinctive pattern in this interval is the precession-obliquity interference in the insolation maxima between 6.55 and 6.43 Ma, which corresponds to the 405-kyr eccentricity minimum around 6.5 Ma. The interference pattern is clearly reflected in the sonic and inductivity logs of the Casanieves borehole and in the thickness of the diatomite beds in the Falconara section on Sicily (T22–28; see Hilgen and Krijgsman, 1999) (Fig. 3). As far as the Upper Abad is concerned, cycles UA8, 10 and 12 usually contain the thickest and most prominent sapropels, where the sapropels of UA9, UA11 and UA13 are less distinct and thinner, with UA13 being thinnest (Sierro et al., 2001). However, this pattern, which fits that of the insolation maxima (Fig. 3), is not always consistent between parallel sections of the Upper Abad. It is also lithologically not evident in the Messadit section in Morocco, where sapropels are not developed, probably as a consequence of the relatively shallow depth of deposition.

In contrast to lithology, the interference pattern is clearly reflected in quantitative planktonic foraminiferal records of the Upper Abad especially in the warm/cold ratio and number of planktonic foraminifers per

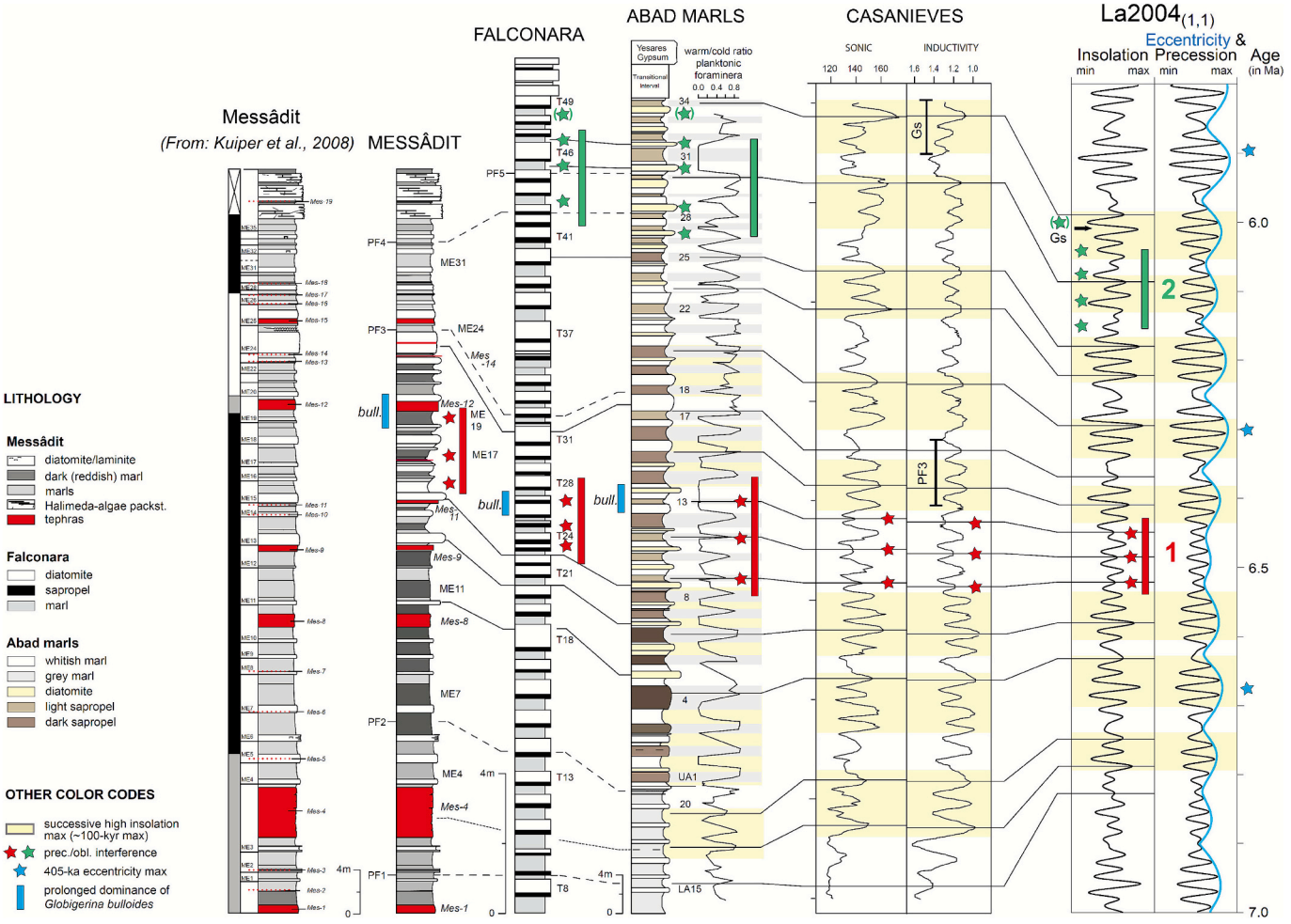

Fig. 3. Integrated stratigraphic correlations between the Messadit, Falconara and Abad marl sections in the Mediterranean and the sonic and inductivity logs of the Casanieves borehole in the Guadalquivir basin of Spain, and the astronomical tuning of these sections and logs to precession and insolation target curves of solution La2004$_{(1,1)}$ for the interval between 6.8 and 6.0 Ma. Dashed lines mark planktonic foraminiferal biostratigraphic correlations between the Mediterranean sections in stratigraphic order: PF1) First Occurrence of *Globorotalia nicolae*, PF2) Last Occurrence of *G. nicolae*, PF3) s/d coiling change of neogloboquadrinids, PF4) first sinistral influx of neogloboquadrinids, and PF5) second sinistral influx of neogloboquadrinids. Black vertical bars mark the interval position of Planktonic foraminifer bioevents in the Casanieves borehole. Gs = Last common occurrence of dextral *Globorotalia scitula*. Lower blue bar labeled *bull.* marks prolonged interval dominated by *Globigerina bulloides*. Red bar (I) marks 405-kyr eccentricity minimum around 6.5 Ma marked by precession-obliquity interference indicated by red stars. Upper green bar (II) marks next younger 405-kyr eccentricity minimum around 6.1 Ma, with precession-obliquity interference indicated by green stars. Sedimentary cycle numbers have been indicated per section. Volcanic ash layers in the Messadit section are indicated in red and the most important ones have been labeled (Mes code). (For interpretation of the references to colour in this figure legend, the reader is referred to the web version of this article.)

gram (Sierro et al., 1999; see Fig. 3). A warm water signal is completely absent in the thin sapropel of UA13 that corresponds to the youngest and weakest insolation maximum in the interference pattern. This results in a prolonged interval in which faunas are dominated by the cold water species *Globigerina bulloides*. This so-called *bulloides* interval is recorded in all key sections at the anticipated position based on the integrated magneto-, bio- and cyclostratigraphic correlations (Fig. 3). The sapropels of cycles UA9 and UA11 that correspond to reduced insolation maxima in the interference pattern do not show a full return to warm water faunas either (Sierro et al., 1999). This faunal pattern is also recognizable at Messadit confirming our previous correlations and tuning (Van Assen et al., 2006). The tuning of this interval marked by precession-obliquity interference in the 405-kyr eccentricity minimum at 6.5 Ma is further consistent with the number of cycles from 6.8 Ma upwards (Hilgen et al., 1995).

2.1.3. 6.25–6.00 Ma

Precession-obliquity interference is also observed in the pattern of diatomite beds in the upper part of the Upper Abad encompassing cycles UA26 to 31 (or even 33, see Sierro et al., 2001). Distinct to prominent diatomite beds are present in UA26, 28, 30 and 31, while such beds are less distinct (UA29) or absent (UA27, lower part UA31) in between. They follow the interference pattern observed in the insolation minima with prominent diatomite beds of UA28 and 30 related to the strongest minima in the middle part of this interval (Fig. 3).

The missing homogeneous marls and diatomite in cycle UA31 results in the very thick sapropel of UA31, implying that this cycle represents a double cycle (Sierro et al., 2001). Sapropels of UA26 and 27 similarly appear as a thick brown layer in the field, but are separated by a thin homogenous marl, while the sapropels of UA28 and 29 are separated by a more distinct homogenous marl, including a diatomite, as expected on the basis of the tuning and the insolation target. The distinctive interference pattern is also recorded by the homogeneous marls of cycles T43-T47 in sections of the Tripoli Fm on Sicily (Falconara in Fig. 3; Hilgen and Krijgsman, 1999). Similar to the correlative cycle UA31 of the Upper Abad, cycle T46 represents a double cycle in which the younger homogeneous marl is supposedly missing (Fig. 3). This characteristic interval is associated with the 405-kyr eccentricity minimum

centered around 6.1 Ma, and is sandwiched between intervals in which the cycles (UA23–26, UA32–34; T37–41, T47–49) reveal a more regular pattern.

The observed phase relation between diatomites in the uppermost Abad and summer insolation minima is consistent with the occurrence of opal CT (microcrystalline silica composed of cristobalite and tridymite) derived from biogenic silica in the homogeneous carbonate-rich marls of the Lower Abad (Sierro et al., 2001). Diatomites of cycles ME32–34 in the Messadit section follow the interference pattern of the Upper Abad diatomites at the onset of the 405-kyr minimum around 6.1 Ma, but no diatomites are found in the younger cycles, due to the abrupt transition to limestone intercalations. By contrast, diatomites in the Tripoli Formation on Sicily show an opposite phase relation with insolation across the 405-kyr eccentricity minimum around 6.5 Ma (Pérez-Folgado et al., 2003), with the thickness of the diatomite beds following the pattern in the insolation maxima (Fig. 3). For the moment, this opposite phase relation is not understood, but Upper Abad cycles are different as they show an extra homogeneous marl in between sapropel and diatomite.

2.2. Statistical evaluation

It has repeatedly been commented that lack of quantitative proxy data (e.g. $\delta^{18}O$) hampers (assessment of) the reliability of the tuning and that statistical tests are needed to evaluate its correctness (see Sinnesael et al., 2019 for the various approaches in cyclostratigraphy). Lithology itself is a proxy for climate change in cyclic successions and nowadays lithology related parameters such as colour and magnetic susceptibility are often measured by default for time series analysis in order to test the presence of Milankovitch cycles and the correctness of a tuning. A limitation of time series analysis of paleoclimate records is the distortion that is inherent to sedimentary successions and related to changes in sedimentation rate, bioturbation, non-linear responses, etc.; this distortion affects the significance levels of spectral peaks (Ripepe and Fischer, 1991; Herbert, 1994; Hilgen et al., 2015). Nevertheless, suitable statistical tools have been developed over the years, such as the average spectral misfit (Meyers and Sageman, 2007) and assessment of amplitude relationships (Meyers, 2015, 2019; Zeeden et al., 2015, 2019), to test for the correctness of a tuning.

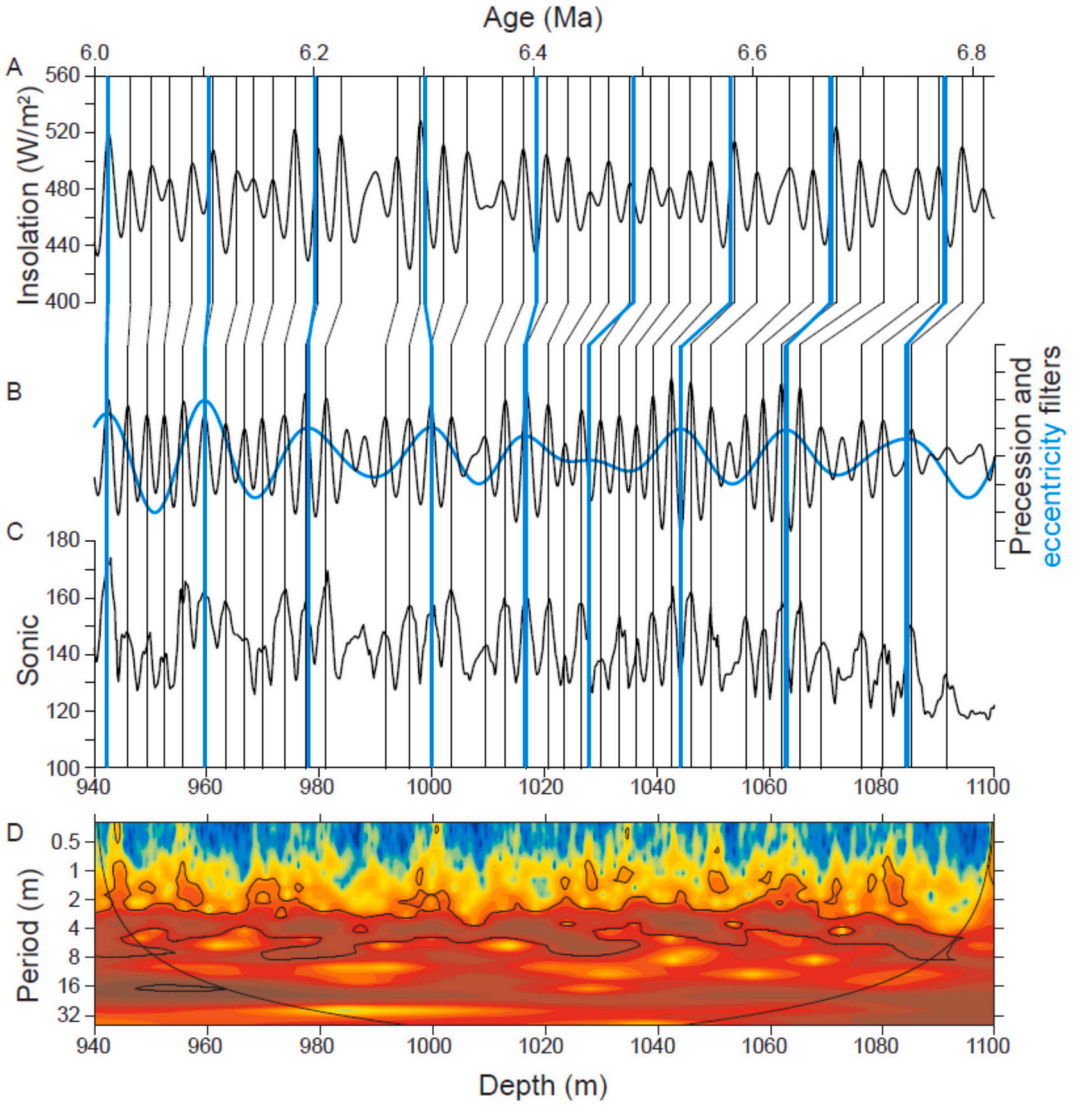

Fig. 4. Wavelet spectrum, the sonic depth record, the bandpass filtered 3–4 and 20 m cycles of the sonic record of the Casanieves borehole (A-C) tuned to the La2004 insolation curve (Laskar et al., 2004). D: The filtered components supposedly reflect precession (3–4) and ~ 100-kyr eccentricity (20 m) cycles and were used for tuning and the independent test of the tuning. Note the dark red power maxima ("blobs") in the 3–4 m band of the wavelet spectrum, which correspond to ~100-kyr eccentricity maxima, the strong signal in the 20 m band related to short ~100-kyr eccentricity and the intermittent presence of an 8 m obliquity related cycle. (For interpretation of the references to colour in this figure legend, the reader is referred to the web version of this article.)

Here we use the Casanieves sonic record to which the Mediterranean sections are correlated at the precession scale, to test the tuning (see Table S1 for data). Spectral analysis in the depth domain revealed peaks with cycle thickness of 20 and 7.6 m, and multiple peaks between 4.4 and 3.3 m. We bandpass filtered the 20 and 4.4–3.3 m cycles, as these should correspond to the ~100 kyr eccentricity cycle and precession (Fig. 4). The filtered 20 m cycle neatly picks up the bundles of 4–5 high amplitude precession related cycles that supposedly reflect the expression of the ~100-kyr eccentricity cycle. An extra cycle is recognized in the interval around 1030 m with the precession-obliquity interference pattern associated with the 405-kyr minimum around 6.5 Ma, in agreement with the eccentricity curve. The amplitude of the filtered precession signal traces the same bundling and also reveals the precession-obliquity interference pattern. This outcome is consistent with the results of wavelet analysis (Fig. 4). The latter reveals enhanced power in the precession frequency band (3–5 m) when the amplitude of the precession related signal is amplified in the well-defined bundles associated with ~100-kyr eccentricity maxima, a strong signal in the ~100-kyr eccentricity band (20 m) and an intermittent presence of an 8 m obliquity related cycle.

We then tested the tuning by looking at the amplitude modulation of the precession signal in the sonic record. The method of using this amplitude modulation to independently test an astronomical tuning has seen a number of improvements over the years to overcome the criticism that the modulation may be an artefact of the tuning itself. The methods of Zeeden et al. (2015, 2019) account for possible tuning artifacts from random data. On the precession scale, we tested four tuning options: the tuning shown in Figs. 3 and 4 that was employed by Kuiper et al. (2008) and Rivera et al. (2011) to calculate their respective astronomically calibrated ages of 28.201 and 28.172 Ma for the FCs, a one precession related insolation cycle younger and older tuning, and a 3 cycles younger tuning. The one cycle older tuning would essentially be consistent with the FCs age of Renne et al. (2011), while a one (or two) and three cycle younger tuning would correspond to Westerhold et al. (2015) and Drury et al. (2017), and to Channell et al. (2010) and Westerhold et al. (2012), respectively. Evaluation of the four tuning options (Fig. 5) was done by comparing robust amplitude variations of the precession signal in the tuned sonic time series (i.e., those not affected by tuning; see Zeeden et al., 2015, 2019) with short term eccentricity from the La2004 solution (Laskar et al., 2004).

The previously published tuning is not only visually compelling, but also statistically highly significant reaching a significance level of 99.88 % for correspondence between the precession amplitude in the sonic data and eccentricity in the astronomical solution (Fig. 5, first column of figures). The one cycle younger tuning results in a considerably lower *P* value, but is still significant at 96.25 % (Fig. 5, fourth column). In fact cross-correlation between the sonic data and La2004 reveals a best fit between the two curves if the precession amplitude of the sonic time series is shifted 4 kyr younger compared to our original tuning. This suggests that the methods developed by (Zeeden et al., 2015) can

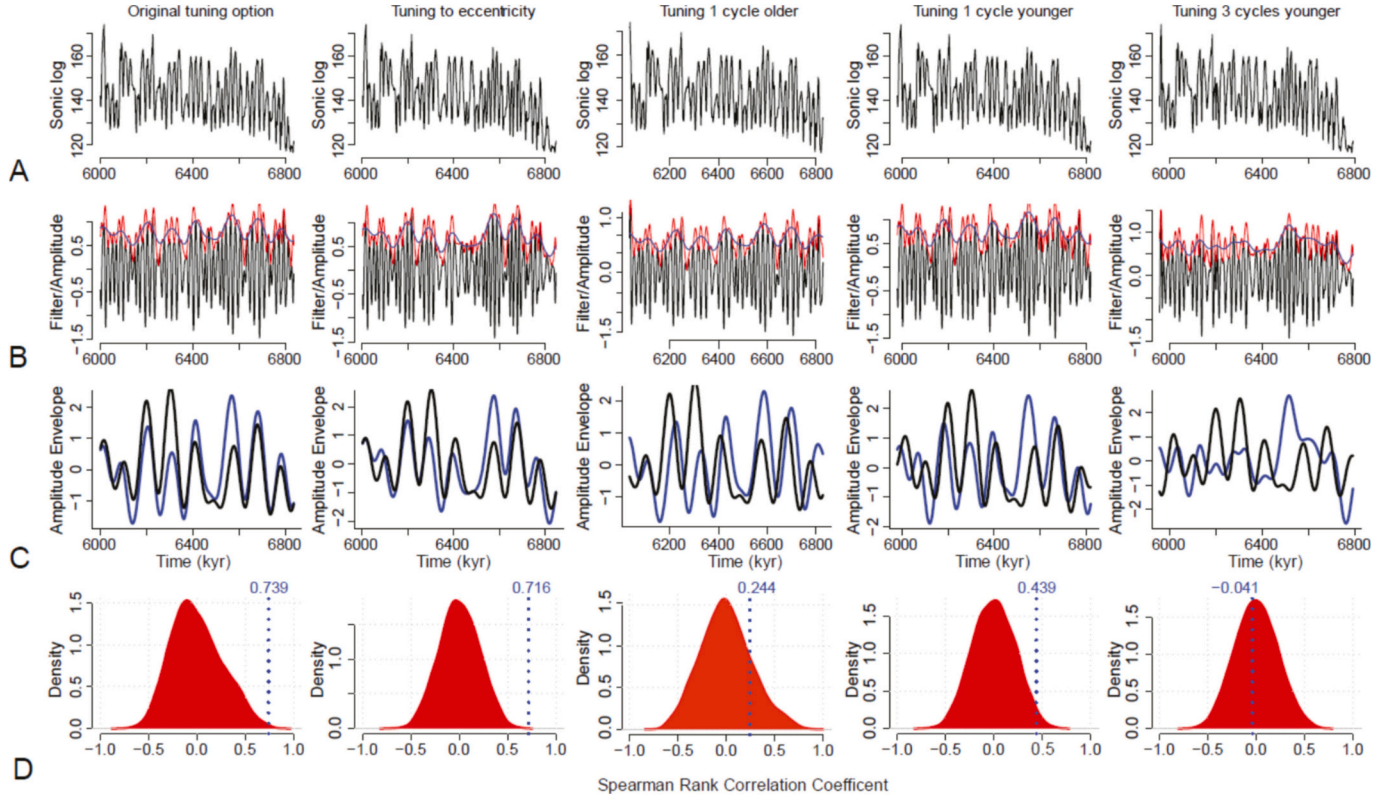

Fig. 5. Evaluation of the astronomically-tuned sonic record from the Casanieves borehole. (A) Sonic time series based on different tunings. Left: tuned time series based on the original tuning followed to the right by tuning to eccentricity that is consistent with the original tuning. Further to the right: time series based on shifting the original tuning one precession cycle older, and one and three precession cycles younger consistent with alternative FCs ages. (B) Sonic record filtered with a broad precession filter (black), its instantaneous amplitude (red), and the final amplitude envelope following application of a lowpass filter (blue). (C) Comparison of the final tuned sonic amplitude envelope (blue) and the amplitude envelope for climatic precession (black; processed using the same filtering algorithm). For plotting purposes, all data series have been standardized (zero mean, unit standard deviation). (D) Kernel density estimate of Spearman rank correlation coefficients for phase-randomized surrogate simulations of the datasets (for more details on the method see Zeeden et al., 2015), and the observed correlation coefficient for the Casanieves sonic tuned record (blue line). Only for the original tuning a distinguishable higher correlation than for the surrogate series is achieved. Prior to analysis, data were interpolated at 1 kyr resolution, which is lower than average data resolution (~0.8 kyr, minimum ~1.1 kyr). Please note that the significance test uses simulations, and will therefore naturally vary between evaluations. Here 10,000 surrogates were tested. (For interpretation of the references to colour in this figure legend, the reader is referred to the web version of this article.)

distinguish between tuning options shifted by one precession cycle, although results depend on, among others, the signal/noise ratio and sampling resolution. The P value for the one cycle older tuning is again markedly lower and the same is true for its significance (Fig. 5, third column). A 2 cycle younger tuning that was not tested would have resulted in a further lowering of the P value and the significance level compared to the one cycle younger tuning. Finally, the 3 cycle younger tuning does not produce a significant relation of the precession amplitude in the resultant sonic time series with eccentricity (Fig. 5, fifth column). This is not surprising as the amplitude now becomes partly opposite to eccentricity, while an opposite phase relation with eccentricity is unlikely. Thus the outcome of this independent test confirms our tuning of the Casanieves borehole and, as a consequence, of the sections in the Mediterranean (Fig. 3). Note that this is also the case if only one tie-point per ~100-kyr cycle is used for the tuning (Fig. 5, second column). Remarkably, this even produces a higher level of significance (99.99 %) than the preferred precession scale tuning.

Another uncertainty in the tuning is the selection of values for tidal dissipation and dynamical ellipticity in the solution. These Earth parameters affect precession and obliquity frequencies and, thus, the precession-obliquity (p-o) interference patterns used to check the validity of the tuning. The $La2004_{(1,1)}$ solution with present-day values for tidal dissipation and dynamical ellipticity was used for tuning the critical interval containing the ash layers for the intercalibration studies. This solution provides an excellent fit with p-o interference patterns observed in the Mediterranean Pliocene and lower Pleistocene, and in the interval between 7.5 and 6 Ma (Figs. 2 and 3). Statistical comparison of quantitative colour proxy records of sapropel-bearing sequences and astronomical target curves for varying values of the tidal dissipation showed that the La2004 solution is reliable back to ~10 Ma (Zeeden et al., 2014). However, a numerical modeling effort recently suggested that the tidal dissipation should already have been reduced to half its present-day value at 3 million years ago (Green et al., 2017), which is in disagreement with the outcome of the cyclostratigraphic analysis (Zeeden et al., 2014). In addition, the role of dynamical ellipticity, the other important parameter, has to be taken into account. However, determining the dynamical ellipticity value is not straightforward, although progress has been made from a modeling perspective (Farhat et al., 2022). The direct tuning of sapropels to boreal summer insolation or, alternatively, to low-latitude inter-hemispheric insolation maxima is validated by the fact that sapropels are generally related to the intensity of the North African summer monsoon. It responds directly and in-phase to the insolation forcing in absence of a strong glacial cyclicity (Weber and Tuenter, 2011; Bosmans et al., 2015; Marzocchi et al., 2015; Grant et al., 2016).

2.3. Summary

Summarizing, we carefully reviewed and explained the details of the tuning of the pre-evaporitic Messinian in the Mediterranean (i.e. between 7.25 and 6.00 Ma). The tuning is constrained by eccentricity and precession-obliquity interference patterns in the lithological cycles and faunal patterns; these are in very good to excellent agreement with the $La2004_{(1,1)}$ target curve, as confirmed by statistical analysis. Therefore, the agreement in intricate cycle patterns present in both the geological record and the insolation curve confirms that the tuning is reliable down to the individual precession cycle. It is not possible to shift the tuning 2–4 precession cycles upward as suggested by Westerhold et al. (2012, 2015) and Drury et al. (2017) without the loss of the excellent fit. This is not surprising as such a shift would result in an opposite phase relation with ~100-kyr eccentricity, which is incompatible with the observed cycle patterns. Also the one precession cycle older tuning, which would be in agreement with the FCs calibration of Renne et al. (2011), leads to a significant reduction in the fit and significance. Detailed calibration studies, using the Faneromeni A1 and MES-4 ash beds (Rivera et al., 2011; Phillips et al., 2017, 2022), suggests that the astronomically calibrated FCs age of 28.201 ± 0.046 Ma is slightly too old, although all ages are consistent within uncertainty.

3. New U/Pb zircon ages of the Faneromeni A1 ash layer and FCT

Here we present new U/Pb ages of the Oligo-Miocene that are potentially pertinent to the age of the FCs. In Section 3.1, we will first focus on a new attempt to apply U/Pb zircon isotopic dating of volcanic ash layers intercalated in deep marine sections of the Mediterranean Miocene to test our astronomical calibration of the FCs. In Section 3.2, we will present new data that are relevant to the direct U/Pb dating of the Fish Canyon Tuff (FCT) itself.

3.1. Faneromeni A1 ash, Crete

The Mediterranean sections discussed in Section 2.1 include the Faneromeni section, which contains the Faneromeni A1 ash layer with an astronomical age of 6.943 Ma (Hilgen et al., 1997; Rivera et al., 2011). Initial attempts to intercalibrate the $^{40}Ar/^{39}Ar$ system with astronomical tuning were based on this ash (Hilgen et al., 1997; Kuiper et al., 2004). This initial intercalibration has been followed by more rigorous approaches (Rivera et al., 2011; Niespolo et al., 2017; Phillips et al., 2017, 2022). The ash layer has been dated by Rivera et al. (2011) and Phillips et al. (2017, 2022) yielding astronomically calibrated ages of respectively 28.172 ± 0.028 Ma (2σ, incl. external errors) (Rivera et al., 2011), 28.187 ± 0.019 Ma (2σ, incl. uncertainties in the reference mineral measurements) (Phillips et al., 2017) and 28.176 ± 0.023 (2σ, incl. external errors) (Phillips et al., 2022) for the FCs (Table 1). The Rivera et al. (2011) calibration incorporates uncertainties associated with the accuracy of the astronomical solution (< 1–2 kyr), lag between insolation and sedimentary expression (< 1 kyr) and assumption of constant sedimentation rate between two astronomically tuned points (< 2 kyr) into account. Rivera et al. (2011) therefore assumes an uncertainty <5 kyr, or better than 0.1 %, in the astronomical age of the volcanic ash layers, while Kuiper et al. (2008) start from a more conservative estimate of ±10 kyr. A critical assumption is that the underlying tuning is correct. Re-assessment of this assumption by carefully checking all relevant cycle patterns, including faunal data of the Abad marls and proxy records from the Casanieves borehole, leads to the conclusion that the initial tuning of these upper Miocene sections is indeed correct (see Section 2).

The A1 ash also contains zircons of which single crystals have been dated in this study. Analytical methods and approaches are described in Wotzlaw et al. (2014) and all data are provided in the supplementary information (Table S2; note that the BSE and CL zircon images in the 2nd and 3rd worksheet of the table are not from the dated zircons themselves, but from other zircon crystals from the A1 ash). Fig. 6 shows single crystal $^{206}Pb/^{238}U$ dates that were corrected for initial ^{230}Th-disequilibrium using a constant Th/U partition coefficient of 0.2 ± 0.1 that results in a correction by 87 ± 11 ka (see Wotzlaw et al., 2014 for details). Th-corrected $^{206}Pb/^{238}U$ dates display substantial excess scatter with single crystal dates ranging from 7.034 ± 0.013 Ma to 6.958 ± 0.016 Ma, but the youngest date overlaps with the astronomical age when considering their respective uncertainties (Fig. 6). The youngest population of statistically equivalent Th-corrected $^{206}Pb/^{238}U$ dates yield a weighted mean date 6.9693 ± 0.0095 Ma (2σ uncertainty, including tracer and decay constant uncertainties), slightly (~1 precession cycle) older than its astronomical age. However, zircons often record complex magmatic histories and the crystals dated here are unlikely to represent the eruption age. To overcome this limitation, Keller et al. (2018) introduced a Bayesian model that estimates the eruption age from complex zircon age distributions. This approach requires some prior estimate of the age distribution, either derived from a priori constraints or from bootstrapping the observed distribution in case of high-*n* datasets. While the true distribution is always unknown, Keller et al. (2018) showed that the model output is insensitive to the choice of the

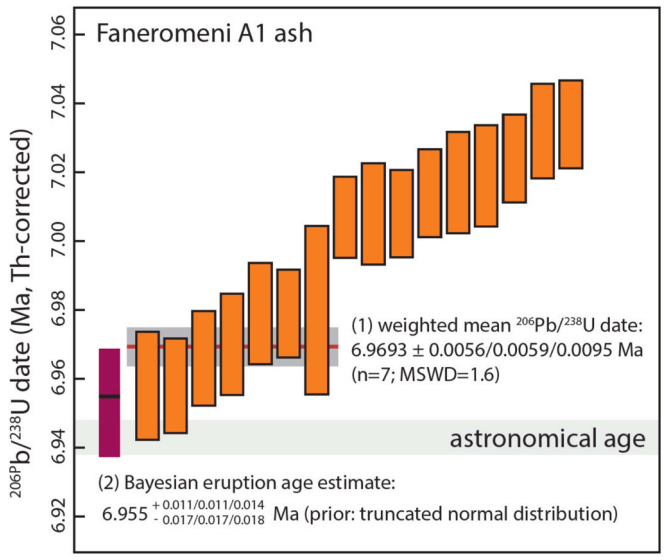

Fig. 6. ^{206}Pb/^{238}U Th-corrected ages for the Faneromeni a1 ash. The weighted mean age is based on the weighted mean ages of the youngest grains with an acceptable MSWD at a given N. Also shown is the Bayesian eruption age based on the Keller et al. (2018) modeling. Astronomical age of the A1 ash layer is shown for reference.

prior distribution. We employed this approach to the A1 zircon U/Pb data assuming a truncated normal distribution as the prior, representing a magmatic zircon crystallization history suddenly interrupted by eruption (Tavazzani et al., 2023), yielding a Bayesian eruption age estimate of 6.955 + 0.14/− 0.18 Ma (including systematic uncertainties associated with the ^{238}U decay constant and the tracer calibration; Jaffey et al., 1971; Condon et al., 2015). This estimate is indistinguishable from the astronomical age, thereby providing independent evidence for the accuracy of the astronomical tuning of the Faneromeni succession (Fig. 6). Note, that this age excludes a 2–3 precession younger tuning of the Faneromeni section necessitated by the – much – younger astronomical calibrations of the FCs, but allows a one precession older tuning in line with the calibration of Renne et al. (2011)

3.2. Fish Canyon tuff

One way to check astronomical calibrations of the FCs is to use U/Pb geochronology to date zircons directly from the Fish Canyon tuff itself. The uncertainty in U/Pb ages is very small (<0.1 %; Schoene et al., 2013). This approach has the great advantage that it will in addition provide a U/Pb age of the FCs without the need of additional steps and assumptions. However, a geological interpretation of magma chamber processes should be taken into account when comparing U/Pb data with the ^{40}Ar/^{39}Ar method. Furthermore, the correction for ^{206}Pb deficit through initial ^{238}U/^{230}Th disequilibrium is an extra source of uncertainty for U/Pb data of late Cenozoic age.

Zircon and titanite of the Fish Canyon Tuff ignimbrite were initially dated by Schmitz and Bowring (2001), yielding weighted mean ^{206}Pb/^{238}U dates of 28.498 ± 0.035 Ma for zircon and 28.395 ± 0.078 Ma for titanite. Subsequent work by Bachmann et al. (2007) revealed that zircons in the FCT record a protracted crystallization history with single crystal dates ranging from ~28.8 to ~28.0 Ma. Further methodological improvements in the ID-TIMS U/Pb dating technique, such as chemical abrasion (Mattinson, 2005), the introduction of the EARTHTIME tracer solution (Condon et al., 2015) and the potential to obtain both chemical and isotopic information on the same zircon crystal (Schoene et al., 2012) required re-assessment of these data. Wotzlaw et al. (2013) applied this improved methodology and used mass balance modeling of the trace element composition and U/Pb dating to track the evolution of the Fish Canyon magma reservoir. Zircons from the Fish Canyon ignimbrite, the pre-caldera Nutras Creek Dacite and an andesite enclave in late erupted intra-caldera deposits reveal a range in ^{206}Pb/^{238}U dates of ~440 kyr, again indicating prolonged zircon residence times. Systematic variations in the trace element composition of the dated zircons were interpreted to record a large-scale crystallization-remelting cycle within the Fish Canyon magma reservoir. The youngest dated zircon grain yields a Th-corrected ^{206}Pb/^{238}U date of 28.196 ± 0.038 Ma (95 % CI, not including tracer and decay constant uncertainties) Wotzlaw et al., 2013; Table 1). Considering the crystallization-remelting history recorded by the zircons, Wotzlaw et al. (2013) claim that the youngest zircon U/Pb dates closely approximate the eruption age of FCT. This dataset was also used by Keller et al. (2018) to test their Bayesian model yielding a model eruption age of 28.186 ± 0.037 Ma (Table 1). This outcome is largely seen as independent confirmation of the astronomical age of 28.201 ± 0.046 Ma for the FCs, but U/Pb zircon dating of the FC tuff also provides a way to directly calibrate the FCs age by means of U/Pb dating.

Notably, the dataset of Wotzlaw et al. (2013) included zircon U/Pb data for a co-erupted andesite enclave extracted from late-erupted intra-caldera ignimbrite. These andesite enclaves were interpreted to sample the andesitic recharge magma that underplated the Fish Canyon magma reservoir which triggered remelting of the crystal mush (Bachmann et al., 2002; Wotzlaw et al., 2013). Somewhat surprisingly, zircon from the andesite enclave yielded a similar range in U/Pb dates as zircon from the Fish Canyon dacite instead of only recording the recharge interval. Since publication of this data in 2013, novel analytical protocols were developed that now permit a more detailed characterization of zircon crystals prior to ID-TIMS analysis using CL imaging and in-situ trace element analysis by laser ablation ICP-MS (e.g., Rivera et al., 2013, 2014; Wotzlaw et al., 2018; Szymanowski et al., 2019) and higher precision U/Pb age determinations (Von Quadt et al., 2016; Wotzlaw et al., 2017) (Table S3).We used these advanced analytical protocols to reassess the U/Pb systematics of zircon from the same andesite enclave analyzed by (Wotzlaw et al., 2013; MLX; Fig. 7A). Zircon crystals were mounted in epoxy, polished to expose their interiors for CL imaging and LA-ICPMS analysis. CL images reveal two distinct populations of zircons – one population with typical magmatic oscillatory zoning and superimposed sector zoning and another population with planar and patchy textures typical of zircon from mafic rocks (Corfu et al., 2003; Karakas et al., 2019; Fig. 7B). The oscillatory zoned crystals strongly resemble zircons from the Fish Canyon dacite and are tentatively interpreted as assimilated antecrysts from the Fish Canyon mush in which the andesite was injected. This is confirmed by their trace element composition which is also equivalent to the dacite zircons with, for instance, low Ti and low Th/U (Fig. 7C and D). In contrast, the zircons with planar and patchy CL textures have systematically higher Ti and higher Th/U consistent with a more mafic host magma. Based on these data, these zircons are interpreted as autocrysts that crystallized from the andesitic recharge magma before or after injection in the Fish Canyon dacite mush. This interpretation is further substantiated by the distinct U/Pb systematics between the two zircon populations. The zircons interpreted as antecrysts yield crystallization ages with a range similar to zircon from the Fish Canyon and Nutras Creek dacites (Wotzlaw et al., 2013). The zircons interpreted as autocrysts from the MLX andesite yield a much narrower range in crystallization ages between 28.292 ± 0.020 Ma and 28.179 ± 0.032 Ma. While the petrologic implications of this data are beyond the scope of this paper, the U/Pb dates of the andesite zircons are very relevant for assessing the calibrations of FCs and this is the focus of our following discussion.

Notably, only the oldest two single crystal zircon dates overlap with the calibration of Renne et al. (2011) while all of the remaining nine dates are within the uncertainty envelope of the Kuiper et al. (2008) calibration (Fig. 7A). This already strongly suggests that the Renne et al. (2011) calibration yields an age for FCs that is significantly too old. The youngest population of zircons with statistically equivalent ^{206}Pb/^{238}U

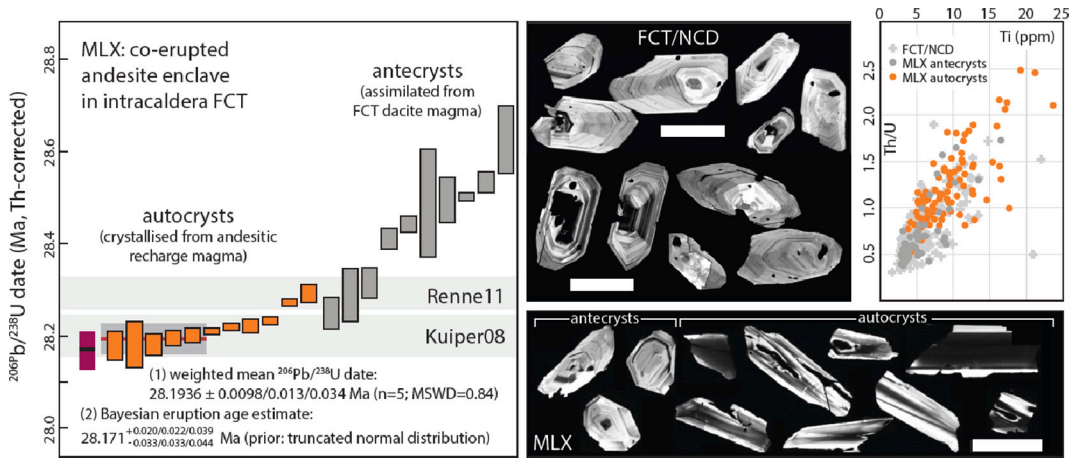

Fig. 7. A. $^{206}Pb/^{238}U$ Th-corrected ages for zircon grains of the MLX co-erupted andesite enclave in the FCT. Distinction is made between autocrysts and antecrysts. Also shown are the calibrations of Kuiper et al. (2008) and Renne et al. (2011) (grey horizontal bars) of the FCs. B. CL images of the two distinct populations of zircons – one population with typical magmatic oscillatory zoning and superimposed sector zoning and another population with planar and patchy textures typical of zircon from mafic rocks. C and D. Trace element composition of the same crystals. Composition of the oscillatory zoned crystals strongly resemble zircons from the Fish Canyon dacite tentatively interpreted as antecrysts with, for instance, low Ti and low Th/U. In contrast, the zircons with planar and patchy CL textures have systematically higher Ti and Th/U consistent with a more mafic host magma. These are interpreted as autocrysts (see running text).

dates yields a weighted mean of 28.194 ± 0.034 Ma (2σ) and using the Bayesian approach of Keller et al. (2018) we derive an eruption age estimate of 28.171 + 0.039/− 0.044 Ma (2σ, including systematic uncertainties) (Table 1). These two dates are in very good agreement with the calibration of Kuiper et al. (2008) and may even point towards a slightly younger eruption age for the Fish Canyon Tuff that is in remarkable agreement with the more recent calibrations of Rivera et al. (2011), Phillips et al. (2017, 2022), and the recently published Bayesian calibration of Carter et al. (2025). This reassessment of the zircon U/Pb systematics of the co-erupted andesite enclave therefore strongly argues for abandoning the Renne et al. (2011) calibration as well as the younger astronomical calibrations and adopting an age of ~28.2 Ma or slightly younger for the FCs.

4. Discussion and future developments

4.1. Discussion

In 2018, geochronologists at the EARTHTIME 2 workshop held in Indianapolis agreed that "*improving the calibration of FCs and other standards via a new series of $^{238}U/^{206}Pb$ and $^{40}Ar/^{39}Ar$ measurements that can be used in the optimization approach of* Renne et al. (2011) *is a goal for both the $^{40}Ar/^{39}Ar$ and $^{238}U/^{206}Pb$ communities (see also,* Reiners et al., 2017*)*" (Schmitz et al., 2020). This will result in an improved intercalibration of $^{40}Ar/^{39}Ar$ and U/Pb dating and a critical test for the U/Pb calibration and optimization of the FCs age of 28.294 Ma of Renne et al. (2011). However, in the meantime, a different innovative approach has been published that uses a Bayesian calibration of the K decay scheme, including Ar/Ar dating, and the U/Pb system (Carter et al., 2025). This resulted in an age of 28.183 ± 0.070 Ma (2σ, full uncertainty) for the FCs (Carter et al., 2025). At the same time, significant progress has been made in determining the U/Pb ages of the FCT by providing relevant new data and analyses (this paper), which resulted in an FCT eruption age of 28.171 ± 0.039/−0.044 Ma.

Our new single crystal U/Pb zircon FCT age and the results of our statistical evaluation of the tuning, on which the astronomically calibrated FCs age of 28.201 Ma is based, show that both the - much - younger astronomical FCs calibrations, varying between 27.89 and 28.10 Ma, as well the older U/Pb based calibration(s) of 28.294 and 28.393 Ma are not correct. In particular, the FCT age of 28.172 ± 0.028 Ma is inconsistent at 2 sigma uncertainty with the optimization age of 28.294 ± 0.036 Ma provided by Renne et al. (2011). The previous FCT age of 28.196 ± 0.038 Ma of Wotzlaw et al. (2013) and the astronomically calibrated FCs age of 28.201 ± 0.046 Ma (Kuiper et al., 2008) were still marginally consistent with that of the Renne et al. (2011) calibration, reason why the latter age continued to be used even though the age of 28.201 Ma was recommended and incorporated in GTS2012 and GTS2020. However, the Rivera et al. (2011) and Phillips et al. (2022) FCs calibrations were already inconsistent with Renne et al. (2011) at the time.

Despite the progress, the fundamental issue of the FCs age has not been completely solved although the much younger astronomical and older U/Pb based ages can now be confidently excluded. However, the question remains what age should be recommended for the FCs in the future and for incorporation in the next standard GTS, in other words should we stick to the astronomically calibrated age of 28.201 ± 0.046 Ma of Kuiper et al. (2008), the preferred FCs age of GTS2012 and GTS2020 (Schmitz, 2012; Schmitz et al., 2020), or switch to a slightly younger age of 28.17–28.18 Ma, although all these ages are consistent at 2σ uncertainty with one another.

For our discussion, it is important to realize that the 28.201 ± 0.046 Ma is based on combining two subsets of data from different laboratories, the Vrije Universiteit Amsterdam (VU) and the Berkeley Geochronology Centre (BGC) (see Kuiper et al., 2008). The ages of 28.184 ± 0.016 / 0.044 Ma (analytical / full uncertainty; BGC) and 28.225 ± 0.019 / 0.044 Ma (analytical / full uncertainty; VU) Ma of these subsets are only marginally consistent and some interlaboratory bias cannot be excluded. Phillips et al. (2022) also used the Moroccan MES-4 ash bed resulting in an age of 28.179 ± 0.010 / 0.042 Ma (analytical / full uncertainty), younger than the VU data, but overlapping with BGC.

Importantly, the younger ages of 28.171–28.176 Ma (Rivera et al., 2011; Phillips et al., 2022; this paper) are inconsistent with the older, 28.225 ± 0.019 / 0.044 Ma, of these two ages at the 1σ uncertainty level. Excluding this older age results in remarkable convergence of FCs ages between 28.171 and 28.184 Ma (see Table 1). In addition, these ages are all calculated with the Min et al. (2000) decay constant. Use of the Steiger and Jäger (1977) decay constant yields in slightly younger ages (e.g., 28.201 Ma vs 28.198 Ma), showing that decay constant uncertainties have a negligible effect on calculated FCs ages.

Several options exist if we aim to select an FCs age for incorporation in the next GTS that is slightly younger than 28.201 Ma. An excellent candidate is the eruption age of 28.171 + 0.039/− 0.044 Ma for the FCT based on the new single crystal U/Pb zircon data presented in this paper

(see Section 3.2). This option has the advantage that the FCs age is directly derived from the Fish Canyon tuff itself and is solely based on the well constrained U/Pb dating system. An alternative option is to start from the astronomically calibrated age of 28.172 ± 0.028 Ma of Rivera et al. (2011) or the related slightly revised age of 28.176 ± 0.023 Ma (Phillips et al., 2022); the latter age also takes the Faneromeni A1 into account while application of the Moroccan MES-4 ash beds results in a slightly older age of 28.179 ± 0.042 Ma with a larger uncertainty. Finally, the 28.813 ± 0.070 Ma of Carter et al. (2025) provides another alternative although, like with the optimalization approach of Renne et al. (2011), the choice of the Ar/Ar-U/Pb age pairs is a point of discussion and the full uncertainty is relatively large. The Carter et al. (2025) approach uses Bayesian statistics combined with Ar/Ar and U/Pb age pairs taken from the Pleistocene to Proterozoic samples to generate Bayesian posterior estimates for ^{40}K and also the ^{238}U and ^{235}U decay constants. This new approach appears to enable the calculation of an FCs age which is in good agreement with the new U/Pb age generated here however the model can only be as good as the data that are included in it, and the assumptions that have been applied. For example, the U/Pb data used for the age pairs are from zircon measurements which come from samples with clear inherited zircon populations (Mitchell III, 2014). This U/Pb age distribution may bias the U/Pb data to older ages, and may also present difficulties in correctly identifying autocrystic and antecrystic zircon crystals which would further biases U/Pb data to older ages (e.g. Claiborne et al., 2010; Schaltegger and Davies, 2017). The Carter et al. (2025) model attempts to deal with these biases in the U/Pb (and Ar/Ar) data by including a crystal (zircon and feldspar) residence time parameter as a prior in their model assuming a uniform prior residence time between 0 and 500 kyr. This approach is in line with the current best practices in dealing with crystal residence and calculation of eruption ages based on Ar/Ar and U/Pb high precision data (e.g. Keller et al., 2018), however it is limited by the data input into the model. To improve the accuracy of the eruption age calculations for each system, high n datasets ($n > 10$ once inherited grains have been removed) should be used to determine the timing of eruption (e.g., Klein and Eddy, 2023; Nathwani et al., 2025). Also, in-situ information such as CL imagines should be included to assess the structure of the dated zircon, and presence or absence of xenocrystic/antecrystic zircon growth, similar to the approach used here with the MLX andesite enclave (Fig. 7). Future studies targeted on improving the Ar/Ar and U/Pb intercalibration should follow these guidelines to ensure that the intercomparison is based on robust assumptions about the data. Also, the U isotopic composition of zircon can vary (Hiess et al., 2012), and this may generate biases in the U/Pb dataset in certain (older) time periods depending on which types of ages are used. This is also something that should be considered in follow up studies to the Carter et al. (2025) work.

4.2. Future developments

4.2.1. Ar/Ar dating: first-principles approach

An alternative to the astronomical and U/Pb calibrations remains the first-principles approach based on the K/Ar method itself. The first principles method for determining the age of standards involves measurement of their ^{40}K and ^{40}Ar* abundances. Morgan et al. (2011, 2023) developed a pipette system, that emits calibrated quantities of ^{40}Ar* via the ideal gas law, to calibrate the sensitivity of the system across a range of source pressures and to estimate the ^{40}Ar* abundances in standards. ^{40}Ar* abundances of HD-B1 and MD2 (GA1550) biotite standards were combined with existing ^{40}K abundance data for these neutron fluence monitors. Ages for fluence monitors were then calculated and combined with intercalibration data for HD-B1 and Fish Canyon sanidine (FCs) to determine ages for FCs (Morgan et al., 2023). These latest results do not yet approach the accuracy of other calibrations, but a number of potential improvements (e.g. choice of material, amount of material gas cleaning procedures) suggests that a revised methodology can be used to make reliable measurements in the future (Morgan et al., 2023). The potential precision attainable by methods described in Morgan et al. (2023) results in significant improvement in age uncertainties due to ^{40}Ar abundance uncertainties. If applied to future determinations of other parameters, such as the electron capture branch of the ^{40}K decay constant via ^{40}Ar ingrowth experiments, this method may independently improve ^{40}Ar/^{39}Ar age uncertainties via multiple pathways (Morgan et al., 2023). This first principles approach should at the end result in an FCs age that is consistent with the astronomical and U/Pb based calibrations.

4.2.2. Intercalibration of astronomical, Ar/Ar and U/Pb dating: triple points and the K/Pg boundary

It is critical that astronomical and U/Pb based calibrations arrive at identical FCs ages. Thus, it is promising that the direct U/Pb zircon dating of the FCT (this paper) and the Bayesian modeling of the K/Ar and U/Pb dating systems (Carter et al., 2025) yielded very similar FCs ages as the astronomically calibrated ages that are favored by the statistical testing of the different tuning options for the cycles in the Mediterranean Miocene (see 2.2). Further testing of this consistency between the three main dating methods used to construct our standard GTS may come from so-called triple points, i.e. stratigraphic horizons or key beds that are suitable for both astronomical as well as single-crystal Ar/Ar sanidine and U/Pb zircon dating. However, such points are uncommon in the Cenozoic with the Faneromeni A1 ash bed being a marked exception. An important older triple point that can be used as testing ground for the intercalibration of the three main dating methods is the K/Pg boundary.

The debate about the astronomical tuning on the long eccentricity scale and age of the K/Pg boundary (e.g., Kuiper et al., 2008; Westerhold et al., 2012) had apparently been solved by radio-isotopic dating of the boundary (Renne et al., 2013; Clyde et al., 2016; Sprain et al., 2018) and by closing the Eocene gap in the astronomical time scale (ATS; Westerhold et al., 2015), resulting in a mutually consistent boundary age of ~66.0 Ma. In particular, the excellent agreement between the Denver basin U/Pb age of 66.021 ± 0.081 Ma (Clyde et al., 2016), the Ar/Ar age of 66.043 ± 0.043 Ma from Montana (Renne et al., 2013; based on Renne et al., 2011) and the astronomical age of 66.020 ± 0.040 Ma (Dinarès-Turell et al., 2014, using La2011) for the boundary looked convincing. Not surprisingly, these ages were incorporated in the Paleogene and Cretaceous chapters of GTS2020 (Gradstein et al., 2020). In the Paleogene chapter, Speijer et al. (2020) used the astronomical age of 66.000 (or 66.001) Ma with reference to Dinarès-Turell et al. (2014), whereas Gale et al. (2020) selected the Ar/Ar age of 66.04 ± 0.05 Ma of Renne et al. (2013), based on the Renne et al. (2011) calibration of the FCs. More recently, the age of Renne et al. (2013) has been replaced by 66.052 ± 0.043 Ma (Sprain et al., 2018), who also used Renne et al. (2011).

Apart from the fact that 40-kyrs, or one obliquity cycle, seems to be missing from the time scale at the K/Pg boundary, the choice of the Ar/Ar age of Renne et al. (2013) starting from the Renne et al. (2011) FCs calibration is remarkable as it is inconsistent with the recommendation to use the astronomically calibrated FCs age of 28.201 ± 0.046 Ma to (re)calculate all Ar/Ar ages in GTS2020 (Schmitz et al., 2020). Hence, the Ar/Ar boundary age of 65.836 ± 0.061 Ma, based on the Kuiper et al. (2008) calibration of Renne et al. (2013) or the slightly revised age of 65.845 ± 0.053 Ma (Sprain et al., 2018) should have been used instead, but these ages would have resulted in a discrepancy of almost 200-kyr with the boundary age in the Neogene chapter. Yet, also our new results for the age of the FCs argue for a discontinuation of the Renne et al. (2011) calibration at 28.294 ± 0.072 Ma.

The preferred K/Pg boundary age following Carter et al. (2025) arrives at 65.799 ± 0.040 Ma (the age shown in their Table 8 has been calculated with the R-value of Swisher III et al. (1993) rather than with the updated R-value of Sprain et al. (2018)). This age falls right in between the boundary ages of 65.778 ± 0.034 and 65.845 ± 0.053 Ma

calculated for the Rivera et al. (2011) and Kuiper et al. (2008) FCs calibrations, when the same R-value is used, but is significantly younger than the corresponding age of 66.052 ± 0.084 Ma according to the Renne et al. (2011) calibration. Yet, such young ages are inconsistent with the astronomical and U/Pb ages of Dinarès-Turell et al. (2014) and Clyde et al. (2016) for the boundary. However, in the meantime, the astronomical age has become younger as well, ranging now from 65.92 to 65.96 Ma (Zeebe and Lourens, 2022). This new astronomical age is based on a detailed comparison of high-resolution climate proxy records with numerous astronomical solutions to overcome the problem of the youngest chaotic transition in the Solar System around 48–50 Ma (Laskar et al., 2011; Zeebe and Lourens, 2019, 2022; Kocken and Zeebe, 2024). Evidently, the ongoing uncertainty about the K/Pg boundary age hampers the final intercalibration of the three main dating methods used to construct the standard GTS.

Summarizing, multi-disciplinary studies of the FCs and especially the K/Pg boundary are needed to guarantee full internal consistency between the main numerical dating methods used to build our GTS and connect Earth's diverse rock archives to reconstruct its intriguing history. However, a crucial step has been made in the right direction with better constraining the FCs age.

5. Conclusions

The tuning of Miocene marine sections in the Mediterranean that underlies the astronomical calibration of the FCs of Kuiper et al. (2008) has been (statistically) evaluated. This evaluation supports the FCs age 28.201 ± 0.046 Ma of Kuiper et al. (2008) and no evidence has been found that the tuning should be 1–3 cycles younger as suggested by Westerhold et al. (2012, 2015) and Drury et al. (2017) or one cycle older as would be consistent with Renne et al. (2011).

Our new U/Pb zircon ages for the FCT are consistent with the astronomically calibrated age of Kuiper et al. (2008), but inconsistent with both much younger astronomical and older U/Pb derived calibrations. The associated Bayesian K18 derived eruption age of the FCT implies a slightly younger age of 28.171 + 0.039/− 0.044 Ma; this age is in excellent agreement with the astronomically calibrated ages of Rivera et al. (2011) and Phillips et al. (2017, 2022), and with the recently published age 28.183 ± 0.070 Ma (Carter et al., 2025), using a Bayesian calibration of the K decay system. It is also in better agreement with the 28.150 Ma of Channell et al. (2020), which is based on the comparison of astronomical and $^{40}Ar/^{39}Ar$ ages for Quaternary magnetic reversals. The K18 derived eruption age has the advantage that it is based on - U/Pb single crystal zircon dating of - the FCT itself.

Finally, the fundamental issue of the age of the FCs seems to be nearly solved as much progress has been made with astronomical and U/Pb calibrations producing almost identical ages. Our recommended age of 28.171–28.176 Ma for the FCs is slightly younger than the 28.201 ± 0.046 Ma that we aimed to test and evaluate. Yet, discrepancies in the K/Pg boundary age have to be solved as well to reach a solid intercalibration of the three main dating methods used to build the standard GTS. More in particular, the intercalibration is critical for attempts to extend the astronomical time scale into the Mesozoic (e.g., Batenburg et al., 2016; Huang, 2018) and potentially into the Paleozoic (e.g., De Vleeschouwer et al., 2012; Wu et al., 2023), and establish for instance the temporal and causal relationship between the volcanic activity of the Deccan Traps and the K/Pg boundary.

CRediT authorship contribution statement

Klaudia F. Kuiper: Writing – review & editing, Writing – original draft, Visualization, Methodology, Funding acquisition, Conceptualization. **Zoë Toorenburgh:** Methodology, Investigation, Formal analysis. **Jörn-Frederik Wotzlaw:** Writing – review & editing, Writing – original draft, Visualization, Validation, Methodology, Investigation, Formal analysis, Conceptualization. **Christian Zeeden:** Writing – review & editing, Writing – original draft, Visualization, Methodology, Investigation, Formal analysis, Conceptualization. **Francisco J. Sierro:** Writing – original draft, Methodology, Investigation, Formal analysis. **Joshua H.F.L. Davies:** Writing – review & editing, Writing – original draft, Visualization, Validation, Methodology, Investigation. **Diana Sahy:** Methodology, Investigation, Formal analysis, Conceptualization. **Daniel J. Condon:** Validation, Methodology, Investigation, Formal analysis. **Frederik J. Hilgen:** Writing - review & editing, Writing - original draft, Visualization, Investigation

Declaration of competing interest

The authors declare that they have no known competing financial interests or personal relationships that could have appeared to influence the work reported in this paper.

Acknowledgements

This work was initiated under European Community's Seventh Framework Program (FP7/2007-2013) under grant agreement number 215458. KK acknowledges the Dutch Research Council (NWO) for financial support under grants 864.12.005 and VI.C.212.103. The authors thank David Szymanowski for help and discussions regarding Bayesian eruption age estimates and propagation of systematic uncertainties

Appendix A. Supplementary data

Supplementary data to this article can be found online at https://doi.org/10.1016/j.palaeo.2025.113421.

Data availability

The authors confirm that all data necessary for supporting the scientific findings of this paper have been provided.

References

Bachmann, O., Dungan, M.A., Lipman, P.W., 2002. The Fish Canyon magma body, San Juan volcanic field, Colorado: rejuvenation and eruption of an upper-crustal batholith. J. Petrol. 43, 1469–1503. https://doi.org/10.1093/petrology/43.8.1469.

Bachmann, O., Oberli, F., Dungan, M.A., Meier, M., Mundil, R., Fischer, H., 2007. $^{40}Ar/^{39}Ar$ and U-Pb dating of the Fish Canyon magmatic system, San Juan Volcanic field, Colorado: evidence for an extended crystallization history. Chem. Geol. 236, 134–166. https://doi.org/10.1016/j.chemgeo.2006.09.005.

Baksi, A.K., Hsü, V., McWilliams, M.O., Farrar, E., 1992. $^{40}Ar/^{39}Ar$ dating of the Brunhes/Matuyama geomagnetic field reversal. Science 256, 356–357. https://doi.org/10.1126/science.256.5055.356.

Batenburg, S.J., De Vleeschouwer, D., Sprovieri, M., Hilgen, F.J., Gale, A.S., Singer, B.S., Koeberl, C., Coccioni, R., Claeys, P., Montanari, A., 2016. Orbital control on the timing of oceanic anoxia in the late Cretaceous. Clim. Past 12, 2009–2016. https://doi.org/10.5194/cp-12-1995-2016.

Bosmans, J.H.C., Hilgen, F.J., Tuenter, E., Lourens, L.J., 2015. Obliquity forcing of low-latitude climate. Clim. Past 11, 1335–1346. https://doi.org/10.5194/cp-11-1335-2015.

Carter, J.N., Hasler, C.E.J., Fuentes, A.J., Tholt, A.J., Morgan, L.E., Renne, P.R., 2025. Bayesian calibration of the 40K decay scheme with implications for 40K-based geochronology. Geochim. Cosmochim. Acta. https://doi.org/10.1016/j.gca.2025.03.024.

Channell, J.E.T., Hodell, D.A., Singer, B.S., Xuan, C., 2010. Reconciling astrochronological and Ar-40/Ar-39 ages, for the Matuyama-Brunhes boundary and late Matuyama Chron. Geochem. Geophys. Geosyst. 11, Q0AA12. https://doi.org/10.1029/2010GC003203.

Channell, J.E.T., Singer, B.S., Jicha, B.R., 2020. Timing of Quaternary geomagnetic reversals and excursions in volcanic and sedimentary archives. Quat. Sci. Rev. 228. https://doi.org/10.1016/j.quascirev.2019.106114 art. no. 106114.

Claiborne, L.L., Miller, C.F., Flanagan, D.M., Clynne, M.A., Wooden, J.L., 2010. Zircon reveals protracted magma storage and recycling beneath Mount St. Helens. Geology 38, 1011–1014. https://doi.org/10.1130/G31285.1.

Clyde, W.C., Ramezani, J., Johnson, K.R., Bowring, S.A., Jones, M.M., 2016. Direct high-precision U-Pb geochronology of the end-Cretaceous extinction and calibration of Paleocene astronomical timescales. Earth Planet. Sci. Lett. 452, 272–280. https://doi.org/10.1016/j.epsl.2016.07.041.

Condon, D.J., Schoene, B., McLean, N.M., Bowring, S.A., Parrish, R.R., 2015. Metrology and traceability of U-Pb isotope dilution geochronology (earthtime tracer calibration part I). Geochim. Cosmochim. Acta 164, 464–480. https://doi.org/10.1016/j.gca.2015.05.026.

Corfu, F., Hanchar, J.M., Hoskin, P.W.O., Kinny, P., 2003. Atlas of zircon textures. Rev. Mineral. Geochem. 53. https://doi.org/10.2113/0530469.

De Vleeschouwer, D., Whalen, M.T., Day, J.E., Claeys, P., 2012. Cyclostratigraphic calibration of the Frasnian (Late Devonian) time scale (Western Alberta, Canada). Bull. Geol. Soc. Am. 124, 928–942. https://doi.org/10.1130/B30547.1.

Dinarès-Turell, J., Westerhold, T., Pujalte, V., Röhl, U., Kroon, D., 2014. Astronomical calibration of the Danian stage (Early Paleocene) revisited: settling chronologies of sedimentary records across the Atlantic and Pacific Oceans. Earth Planet. Sci. Lett. 405, 119–131. https://doi.org/10.1016/j.epsl.2014.08.027.

Drury, A.J., Westerhold, T., Frederichs, T., Tian, J., Wilkens, R., Channell, J.E.T., Evans, H., Johns, C.M., Lyle, M., Rohl, U., 2017. Late Miocene climate and time scale reconciliation: accurate orbital calibration from a deep-sea perspective. Earth Planet. Sci. Lett. 475, 254–266. https://doi.org/10.1016/j.epsl.2017.07.038.

Farhat, M., Laskar, J., Boué, G., 2022. Constraining the Earth's dynamical ellipticity from ice age dynamics. J. Geophys. Res. Solid Earth 127, e2021JB023323. https://doi.org/10.1029/2021JB023323.

Gale, A.S., Mutterlose, J., Batenburg, S.J., Gradstein, F.M., Agterberg, F.P., Ogg, J.G., Petrizzo, M.R., 2020. The Cretaceous period. In: Gradstein, et al. (Eds.), Geologic Time Scale, 2020, pp. 1023–1086. https://doi.org/10.1016/B978-0-12-824360-2.00027-9.

Ganerød, M., Chew, D.M., Smethurst, M.A., Troll, V.R., Corfu, F., Meade, F., Prestvik, T., 2011. Geochronology of the Tardree rhyolite complex, Northern Ireland: implications for zircon fission track studies, the North Atlantic Igneous Province and the age of the Fish Canyon sanidine standard. Chem. Geol. 286, 222–228. https://doi.org/10.1016/j.chemgeo.2011.05.007.

Gradstein, F.M., Ogg, J.G., Schmitz, M.D., Ogg, G.M., 2012. The Geological Time Scale 2012. Elsevier, Boston, p. 1144. https://doi.org/10.1016/C2011-1-08249-8.

Gradstein, F.M., Ogg, J.G., Schmitz, M.D., Ogg, G.M., 2020. Geologic Time Scale 2020. Elsevier, p. 1357. https://doi.org/10.1016/B978-0-12-824360-2.00032-2.

Grant, K.M., Grimm, R., Mikolajewicz, U., Marino, G., Ziegler, M., Rohling, E.J., 2016. The timing of Mediterranean sapropel deposition relative to insolation, sea-level and African monsoon changes. Quat. Sci. Rev. 140, 125–141. https://doi.org/10.1016/j.quascirev.2016.03.026.

Green, J.A.M., Huber, M., Waltham, D., Buzan, J., Wells, M., 2017. Explicitly modelled deep-time tidal dissipation and its implication for lunar history. Earth Planet. Sci. Lett. 461, 46–53. https://doi.org/10.1016/j.epsl.2016.12.038.

Herbert, T.D., 1994. Reading orbital signals distorted by sedimentation: models and examples. In: de Boer, P.L., Smith, D.G. (Eds.), Orbital Forcing and Cyclic Sequences. Blackwell Publishing Ltd., pp. 483–507. https://doi.org/10.1002/9781444304039.ch29

Hiess, J., Condon, D.J., McLean, N., Noble, S.R., 2012. 238U/235U systematics in terrestrial uranium-bearing minerals. Science 335, 1610–1614. https://doi.org/10.1126/science.1215507.

Hilgen, F.J., Krijgsman, W., 1999. Cyclostratigraphy and astrochronology of the Tripoli diatomite Formation (pre-evaporite Messinian, Sicily, Italy). Terra Nova 11, 16–22. https://doi.org/10.1046/j.1365-3121.1999.00221.x.

Hilgen, F.J., Krijgsman, W., Langereis, C.G., Lourens, L.J., Santarelli, A., Zachariasse, W.J., 1995. Extending the astronomical (polarity) time scale into the Miocene. Earth Planet. Sci. Lett. 136, 495–510. https://doi.org/10.1016/0012-821X(95)00207-S.

Hilgen, F.J., Krijgsman, W., Wijbrans, J.R., 1997. Direct comparison of astronomical and Ar-40/Ar-39 ages of ash beds: potential implications for the age of mineral dating standards. Geophys. Res. Lett. 24, 2043–2046. https://doi.org/10.1029/97GL02029.

Hilgen, F.J., Bissoli, L., Iaccarino, S., Krijgsman, W., Meijer, R., Negri, A., Villa, G., 2000. Integrated stratigraphy and astrochronology of the Messinian GSSP at Oued Akrech (Atlantic Morocco). Earth Planet. Sci. Lett. 182, 237–251. https://doi.org/10.1016/S0012-821X(00)00247-8.

Hilgen, F.J., Lourens, L.J., Van Dam, J.A., Beu, A.G., Boyes, A.F., Cooper, R.A., Krijgsman, W., Ogg, J.G., Piller, W.E., Wilson, D.S., 2012. Chapter 29 - the Neogene period. In: Gradstein, et al. (Eds.), The Geologic Time Scale 2012. Elsevier, Boston, pp. 923–978. https://doi.org/10.1016/B978-0-444-59425-9.00029-9.

Hilgen, F.J., Hinnov, L.A., Abdul Aziz, H., Abels, H.A., Batenburg, S., Bosmans, J.H.C., de Boer, B., Hüsing, S.K., Kuiper, K.F., Lourens, L.J., Rivera, T., Tuenter, E., Van de Wal, R.S.W., Wotzlaw, J.-F., Zeeden, C., 2015. Stratigraphic continuity and fragmentary sedimentation: the success of cyclostratigraphy as part of integrated stratigraphy. Geol. Soc. Spec. Publ. 404, 157–197. https://doi.org/10.1144/SP404.12.

Huang, C., 2018. Astronomical time scale for the Mesozoic. In: Montanari, M. (Ed.), Cyclostratigraphy and Astrochronology. Stratigraphy & Time Scales, vol. 3. Academic Press, London, pp. 81–150. https://doi.org/10.1016/bs.sats.2018.08.005.

Jaffey, A.H., Flynn, K.F., Glendenin, L.E., Bentley, W.C., Essling, A.M., 1971. Precision measurement of half-lives and specific activities of U235 and U238. Phys. Rev. C 4, 1889–1906. https://doi.org/10.1103/PhysRevC.4.1889.

Karakas, O., Wotzlaw, J.-F., Guillong, M., Ulmer, P., Brack, P., Economos, R., Bergantz, G.W., Sinigoi, S., Bachmann, O., 2019. The pace of crustal-scale magma accretion and differentiation beneath silicic caldera volcanoes. Geology 47, 719–723. https://doi.org/10.1130/G46020.1.

Keller, C.B., Schoene, B., Samperton, K.M., 2018. A stochastic sampling approach to zircon eruption age interpretation. Geochem. Perspect. Lett. 8, 31–35. https://doi.org/10.7185/geochemlet.1826.

Klein, B.Z., Eddy, M.P., 2023. What's in an age? Calculation and interpretation of ages and durations from U-Pb zircon geochronology of igneous rocks. Geol. Soc. Am. Bull. https://doi.org/10.1130/B36686.1.

Kocken, I.J., Zeebe, R.E., 2024. Testing astronomical solutions with geological data for the latest Cretaceous: an astronomically tuned time scale. Paleoceanogr. Paleoclimatol. 39. https://doi.org/10.1029/2024PA004954 art. no. e2024PA004954.

Krijgsman, W., Hilgen, F.J., Negri, A., Wijbrans, J.R., Zachariasse, W.J., 1997. The Monte del Casino section (Northern Apennines, Italy): a potential Tortonian/Messinian boundary stratotype? Palaeogeogr. Palaeoclimatol. Palaeoecol. 133, 27–47. https://doi.org/10.1016/S0031-0182(97)00039-4.

Kuiper, K.F., Hilgen, F.J., Steenbrink, J., Wijbrans, J.R., 2004. Ar-40/Ar-39 ages of tephras intercalated in astronomically tuned Neogene sedimentary sequences in the eastern Mediterranean. Earth Planet. Sci. Lett. 222, 583–597. https://doi.org/10.1016/j.epsl.2004.03.005.

Kuiper, K.F., Deino, A., Hilgen, F.J., Krijgsman, W., Renne, P.R., Wijbrans, J.R., 2008. Synchronizing rock clocks of Earth history. Science 320, 500–504. https://doi.org/10.1126/science.1154339.

Laskar, J., Correia, A.C.M., Gastineau, M., Joutel, F., Levrard, B., Robutel, P., 2004. Long term evolution and chaotic diffusion of the insolation quantities of Mars. Icarus 170, 343–364. https://doi.org/10.1016/j.icarus.2004.04.005.

Laskar, J., Gastineau, M., Delisle, J.-B., Farrés, A., Fienga, A., 2011. Strong chaos induced by close encounters with Ceres and Vesta. Astron. Astrophys. 532. https://doi.org/10.1051/0004-6361/201117504 art. no. L4.

Ledesma, S., 2000. Astrobiocronología y estratigrafía de alta resolución del Neógeno de la Cuenca del Guadalquivir, Golfo de Cádiz. Universidad de Salamanca, p. 464.

Marzocchi, A., Lunt, D.J., Flecker, R., Bradshaw, C.D., Farnsworth, A., Hilgen, F.J., 2015. Orbital control on late Miocene climate and the North African monsoon: insight from an ensemble of sub-precessional simulations. Clim. Past 11, 1271–1295. https://doi.org/10.5194/cp-11-1271-2015.

Mattinson, J.M., 2005. Zircon U-Pb chemical abrasion ("CA-TIMS") method: combined annealing and multi-step partial dissolution analysis for improved precision and accuracy of zircon ages. Chem. Geol. 220, 47–66. https://doi.org/10.1016/j.chemgeo.2005.03.011.

McDougall, I., Brown, F.H., Cerling, T.E., Hillhouse, J.W., 1992. A reappraisal of the geomagnetic polarity time scale to 4 Ma using data from the Turkana basin, East Africa. Geophys. Res. Lett. 19, 2349–2352. https://doi.org/10.1029/92GL02714.

Meyers, S.R., 2015. The evaluation of eccentricity-related amplitude modulation and bundling in paleoclimate data: an inverse approach for astrochronologic testing and time scale optimization. Paleoceanography 30, 1625–1640. https://doi.org/10.1002/2015PA002850.

Meyers, S.R., 2019. Cyclostratigraphy and the problem of astrochronologic testing. Earth Sci. Rev. 190, 190–223. https://doi.org/10.1016/j.earscirev.2018.11.015.

Meyers, S.R., Sageman, B.B., 2007. Quantification of deep-time orbital forcing by average spectral misfit. Am. J. Sci. 307, 773–792. https://doi.org/10.2475/05.2007.01.

Min, K.W., Mundil, R., Renne, P.R., Ludwig, K.R., 2000. A test for systematic errors in Ar-40/Ar-39 geochronology through comparison with U/Pb analysis of a 1.1-Ga rhyolite. Geochim. Cosmochim. Acta 64, 73–98. https://doi.org/10.1016/S0016-7037(99)00204-5.

Mitchell III, W.S., 2014. High-Resolution U-Pb Geochronology of Terrestrial Cretaceous-Paleogene and Permo-Triassic Boundary Sequences in North America. PhD-thesis. University of California, Berkeley.

Morgan, L.E., Postma, O., Kuiper, K.F., Mark, D.F., van der Plas, W., Davidson, S., Perkin, M., Villa, I.M., Wijbrans, J.R., 2011. A metrological approach to measuring $^{40}Ar^{*}$ concentrations in K-Ar and $^{40}Ar/^{39}Ar$ mineral standards. Geochem. Geophys. Geosyst. 12, A0AA20. https://doi.org/10.1029/2011GC003719.

Morgan, L.E., Davidheiser-Kroll, B., Kuiper, K.F., Mark, D.F., McLean, N.M., Wijbrans, J. R., 2023. First principles calibration of ^{40}Ar abundances in $^{40}Ar/^{39}Ar$ mineral neutron fluence monitors: methodology and preliminary results. Geostand. Geoanal. Res. 47, 91–104. https://doi.org/10.1111/ggr.12464.

Nathwani, C., Szymanowski, D., Tavazzani, L., Markovic, S., Virmond, A.L., Chelle-Michou, C., 2025. Controls on zircon age distributions in volcanic, porphyry and plutonic rocks. Geochronology 7, 15–33. https://doi.org/10.5194/gchron-7-15-2025.

Niespolo, E.M., Rutte, D., Deino, A.L., Renne, P.R., 2017. Intercalibration and age of the Alder Creek sanidine Ar-40/Ar-39 standard. Quat. Geochronol. 39, 205–213. https://doi.org/10.1016/j.quageo.2016.09.004.

Pérez-Folgado, M., Sierro, F.J., Bárcena, M.A., Flores, J.A., Vázquez, A., Utrilla, R., Hilgen, F.J., Krijgsman, W., Filippelli, G.M., 2003. Western versus eastern Mediterranean paleoceanographic response to astronomical forcing: a high-resolution microplankton study of precession-controlled sedimentary cycles during the Messinian. Palaeogeogr. Palaeoclimatol. Palaeoecol. 190, 317–334. https://doi.org/10.1016/S0031-0182(02)00612-0.

Phillips, D., Matchan, E.L., Honda, M., Kuiper, K.F., 2017. Astronomical calibration of Ar-40/Ar-39 reference minerals using high-precision, multi-collector (ARGUSVI) mass spectrometry. Geochim. Cosmochim. Acta 196, 351–369. https://doi.org/10.1016/j.gca.2016.09.027.

Phillips, D., Matchan, E.L., Dalton, H., Kuiper, K.F., 2022. Revised astronomically calibrated 40Ar/39Ar ages for the Fish Canyon Tuff sanidine – closing the interlaboratory gap. Chem. Geol. 597. https://doi.org/10.1016/j.chemgeo.2022.120815 art. no. 120815.

Raffi, I., Wade, B.S., Pälike, H., Beu, A.G., Cooper, R., Crundwell, M.P., Krijgsman, W., Moore, T., Raine, J.I., Sardella, R., Vernyhorova, Y.V., 2020. The Neogene period. In: Gradstein, F., et al. (Eds.), Geologic Time Scale 2020. Elsevier, pp. 1141–1215. https://doi.org/10.1016/B978-0-12-824360-2.00029-2.

Reiners, P.W., Carlson, R.W., Renne, P.R., Cooper, K.M., Granger, D.E., McLean, N.M., Schoene, B., 2017. Geochronology and Thermochronology. John Wiley & Sons, p. 464. https://doi.org/10.1002/9781118455876.

Renne, P.R., Deino, A.L., Walter, R.C., Turrin, B.D., Swisher III, C.C., Becker, T.A., Curtis, G.H., Sharp, W.D., Jaouni, A.-R., 1994. Intercalibration of astronomical and radioisotopic time. Geology 22, 783–786. https://doi.org/10.1130/0091-7613(1994)022<0783:IOAART>2.3.CO;2.

Renne, P.R., Swisher, C.C., Deino, A.L., Karner, D.B., Owens, T.L., DePaolo, D.J., 1998. Intercalibration of standards, absolute ages and uncertainties in Ar-40/Ar-39 dating. Chem. Geol. 145, 117–152. https://doi.org/10.1016/S0009-2541(97)00159-9.

Renne, P.R., Mundil, R., Balco, G., Min, K.W., Ludwig, K.R., 2010. Joint determination of K-40 decay constants and Ar-40*/K-40 for the Fish Canyon sanidine standard, and improved accuracy for Ar-40/Ar-39 geochronology. Geochim. Cosmochim. Acta 74, 5349–5367. https://doi.org/10.1016/j.gca.2010.06.017.

Renne, P.R., Balco, G., Ludwig, K.R., Mundil, R., Min, K., 2011. Response to the comment by W.H. Schwarz et al. on "Joint determination of K-40 decay constants and Ar-40*/K-40 for the Fish Canyon sanidine standard, and improved accuracy for Ar-40/Ar-39 geochronology" by P.R. Renne et al. (2010). Geochim. Cosmochim. Acta 75, 5097–5100. https://doi.org/10.1016/j.gca.2011.06.021.

Renne, P.R., Deino, A.L., Hilgen, F.J., Kuiper, K.F., Mark, D.F., Mitchell, W.S., Morgan, L. E., Mundil, R., Smit, J., 2013. Time scales of critical events around the Cretaceous-Paleogene boundary. Science 339, 684–687. https://doi.org/10.1126/science.1230492.

Ripepe, M., Fischer, A.G., 1991. Stratigraphic rhythms synthesized from orbital variations. J. Sediment. Petrol. 63, 335–344. https://doi.org/10.17161/kgsbulletin.no.233.20466.

Rivera, T.A., Schmitz, M.D., Crowley, J.L., Storey, M., 2014. Rapid magma evolution constrained by zircon petrochronology and 40Ar/39Ar sanidine ages for the Huckleberry Ridge Tuff, Yellowstone, USA. Geology 42, 643–646. https://doi.org/10.1130/G35808.1.

Rivera, T.A., Storey, M., Schmitz, M.D., Crowley, J.L., 2013. Age intercalibration of 40Ar/39Ar sanidine and chemically distinct U/Pb zircon populations from the Alder Creek Rhyolite Quaternary geochronology standard. Chem. Geol. 345, 87–98. https://doi.org/10.1016/j.chemgeo.2013.02.021.

Rivera, T.A., Storey, M., Zeeden, C., Hilgen, F.J., Kuiper, K., 2011. A refined astronomically calibrated Ar-40/Ar-39 age for Fish Canyon sanidine. Earth Planet. Sci. Lett. 311, 420–426. https://doi.org/10.1016/j.epsl.2011.09.017.

Schaltegger, U., Davies, J.H.F.L., 2017. Petrochronology of zircon and baddeleyite in igneous rocks: reconstructing magmatic processes at high temporal resolution. Rev. Mineral. Geochem. 83, 297–328. https://doi.org/10.2138/rmg.2017.83.10.

Schmitz, M.D., 2012. Chapter 6 - radiogenic isotope geochronology. In: Gradstein, F., et al. (Eds.), The Geologic Time Scale 2012. Elsevier, Boston, pp. 115–126. https://doi.org/10.1016/B978-0-444-59425-9.00006-8.

Schmitz, M.D., Bowring, S.A., 2001. U-Pb zircon and titanite systematics of the Fish Canyon Tuff: an assessment of high-precision U-Pb geochronology and its application to young volcanic rocks. Geochim. Cosmochim. Acta 65, 2571–2587. https://doi.org/10.1016/S0016-7037(01)00616-0.

Schmitz, M.D., Singer, B.S., Rooney, A.D., 2020. Radioisotope geochronology. In: Gradstein, et al. (Eds.), Geologic Time Scale 2020. Elsevier, pp. 193–209. https://doi.org/10.1016/B978-0-12-824360-2.00006-1.

Schoene, B., Schaltegger, U., Brack, P., Latkoczy, C., Stracke, A., Günther, D., 2012. Rates of magma differentiation and emplacement in a ballooning pluton recorded by U-Pb TIMS-TEA, Adamello batholith, Italy. Earth Planet. Sci. Lett. 355-356, 162–173. https://doi.org/10.1016/j.epsl.2012.08.019.

Schoene, B., Condon, D.J., Morgan, L., McLean, N., 2013. Precision and accuracy in geochronology. Elements 9, 19–24. https://doi.org/10.2113/gselements.9.1.19.

Sierro, F.J., Flores, J.A., Zamarreno, I., Vazquez, A., Utrilla, R., Frances, G., Hilgen, F.J., Krijgsman, W., 1999. Messinian pre-evaporite sapropels and procession-induced oscillations in western Mediterranean climate. Mar. Geol. 153, 137–146. https://doi.org/10.1016/S0025-3227(98)00085-1.

Sierro, F.J., Hilgen, F.J., Krijgsman, W., Flores, J.A., 2001. The Abad composite (SE Spain): a Messinian reference section for the Mediterranean and the APTS. Palaeogeogr. Palaeoclimatol. Palaeoecol. 168, 141–169. https://doi.org/10.1016/S0031-0182(00)00253-4.

Sinnesael, M., De Vleeschouwer, D., Zeeden, C., Batenburg, S.J., Da Silva, A.-C., de Winter, N.J., Dinarès-Turell, J., Drury, A.J., Gambacorta, G., Hilgen, F.J., Hinnov, L. A., Hudson, A.J.L., Kemp, D.B., Lantink, M.L., Laurin, J., Li, M., Liebrand, D., Ma, C., Meyers, S.R., Monkenbusch, J., Montanari, A., Nohl, T., Pälike, H., Pas, D., Ruhl, M., Thibault, N., Vahlenkamp, M., Valero, L., Wouters, S., Wu, H., Claeys, P., 2019. The Cyclostratigraphy Intercomparison Project (CIP): consistency, merits and pitfalls. Earth-Sci. Revs. 199, 102965. https://doi.org/10.1016/j.earscirev.2019.102965.

Speijer, R.P., Pälike, H., Hollis, C.J., Hooker, J.J., Ogg, J.G., 2020. The Paleogene period. In: Gradstein, et al. (Eds.), Geologic Time Scale 2020. Elsevier, pp. 1087–1140. https://doi.org/10.1016/B978-0-12-824360-2.00028-0.

Spell, T.L., McDougall, I., 1992. Revisions of the age of the Brunhes-Matuyama Boundary and the Pleistocene geomagnetic polarity timescale. Geophys. Res. Lett. 19, 1181–1184. https://doi.org/10.1029/92GL01125.

Sprain, C.J., Renne, P.R., Clemens, W.A., Wilson, G.P., 2018. Calibration of chron C29r: new high-precision geochronologic and paleomagnetic constraints from the Hell Creek region, Montana. GSA Bull. 130, 1615–1644. https://doi.org/10.1130/B31890.1.

Steiger, R.H., Jäger, E., 1977. Subcommission on geochronology - convention on use of decay constants in geochronology and cosmochronology. Earth Planet. Sci. Lett. 36, 359–362. https://doi.org/10.1016/0012-821X(77)90060-7.

Swisher III, C.C., Dingus, L., Butler, R.F., 1993. 40Ar/39Ar dating and magnetostratigraphic correlation of the terrestrial Cretaceous-Paleogene boundary and Puercan Mammal Age, Hell Creek-Tullock formations, eastern Montana. Can. J. Earth Sci. 30, 1981–1996. https://doi.org/10.1139/e93-174.

Szymanowski, D., Ellis, B.S., Wotzlaw, J.-F., Bachmann, O., 2019. Maturation and rejuvenation of a silicic magma reservoir: high-resolution chronology of the Kneeling Nun Tuff. Earth Planet. Sci. Lett. 510, 103–115. https://doi.org/10.1016/j.epsl.2019.01.007.

Tauxe, L., Deino, A.D., Behrensmeyer, A.K., Potts, R., 1992. Pinning down the Brunhes/Matuyama and upper Jaramillo boundaries: a reconciliation of orbital and isotopic time scales. Earth Planet. Sci. Lett. 109, 561–572. https://doi.org/10.1016/0012-821X(92)90114-B.

Tavazzani, L., Wotzlaw, J.-F., Economos, R., Sinigoi, S., Demarchi, G., Szymanowski, D., Laurent, O., Bachmann, O., Chelle-Michou, C., 2023. High-precision zircon age spectra record the dynamics and evolution of large open-system silicic magma reservoirs. Earth Planet. Sci. Lett. 623. https://doi.org/10.1016/j.epsl.2023.118432 art. no. 118432.

Van Assen, E., Kuiper, K.F., Barhoun, N., Krijgsman, W., Sierro, F.J., 2006. Messinian astrochronology of the Melilla Basin: stepwise restriction of the Mediterranean-Atlantic connection through Morocco. Palaeogeogr. Palaeoclimatol. Palaeoecol. 238, 15–31. https://doi.org/10.1016/j.palaeo.2006.03.014.

Von Quadt, A., Wotzlaw, J.-F., Buret, Y., Large, S.J.E., Peytcheva, I., Trinquier, A., 2016. High-precision zircon U/Pb geochronology by ID-TIMS using new 10^{13} ohm resistors. J. Anal. At. Spectrom. 31, 658–665. https://doi.org/10.1039/c5ja00457h.

Weber, S.L., Tuenter, E., 2011. The impact of varying ice sheets and greenhouse gases on the intensity and timing of boreal summer monsoons. Quat. Sci. Rev. 30, 469–479. https://doi.org/10.1016/j.quascirev.2010.12.009.

Westerhold, T., Röhl, U., Laskar, J., 2012. Time scale controversy: accurate orbital calibration of the early Paleogene. Geochem. Geophys. Geosyst. 13, Q06015. https://doi.org/10.1029/2012GC004096.

Westerhold, T., Roehl, U., Frederichs, T., Bohaty, S.M., Zachos, J.C., 2015. Astronomical calibration of the geological timescale: closing the middle Eocene gap. Clim. Past 11, 1181–1195. https://doi.org/10.5194/cp-11-1181-2015.

Wotzlaw, J.F., Schaltegger, U., Frick, D.A., Dungan, M.A., Gerdes, A., Gunther, D., 2013. Tracking the evolution of large-volume silicic magma reservoirs from assembly to supereruption. Geology 41, 867–870. https://doi.org/10.1130/G34366.1.

Wotzlaw, J.F., Hüsing, S.K., Hilgen, F.J., Schaltegger, U., 2014. High-precision zircon U-Pb geochronology of astronomically dated volcanic ash beds from the Mediterranean Miocene. Earth Planet. Sci. Lett. 407, 19–34. https://doi.org/10.1016/j.epsl.2014.09.025.

Wotzlaw, J.-F., Buret, Y., Large, S.J.E., Szymanowski, D., Von Quadt, A., 2017. ID-TIMS U-Pb geochronology at the 0.1‰ level using 10^{13} Ω resistors and simultaneous U and $^{18}O/^{16}O$ isotope ratio determination for accurate UO_2 interference correction. J. Anal. At. Spectrom. 32, 579–586. https://doi.org/10.1039/c6ja00278a.

Wotzlaw, J.-F., Brack, P., Storck, J.-C., 2018. High-resolution stratigraphy and zircon U-Pb geochronology of the middle Triassic Buchenstein Formation (Dolomites, Northern Italy): precession-forcing of hemipelagic carbonate sedimentation and calibration of the Anisian-Ladinian boundary interval. J. Geol. Soc. Lond. 175, 71–85. https://doi.org/10.1144/jgs2017-052.

Wu, H., Fang, Q., Hinnov, L.A., Zhang, S., Yang, T., Shi, M., Li, H., 2023. Astronomical time scale for the Paleozoic era. Earth Sci. Rev. 244. https://doi.org/10.1016/j.earscirev.2023.104510 art. no. 104510.

Zeebe, R.E., Lourens, L.J., 2019. Solar system chaos and the Paleocene–Eocene boundary age constrained by geology and astronomy. Science 365, 926–929. https://doi.org/10.1126/science.aax0612.

Zeebe, R.E., Lourens, L.J., 2022. Geologically constrained astronomical solutions for the Cenozoic era. Earth Planet. Sci. Lett. 592, 117595. https://doi.org/10.1016/j.epsl.2022.117595.

Zeeden, C., Hilgen, F.J., Husing, S.K., Lourens, L.L., 2014. The Miocene astronomical time scale 9-12 Ma: new constraints on tidal dissipation and their implications for paleoclimatic investigations. Paleoceanography 29, 296–307. https://doi.org/10.1002/2014PA002615.

Zeeden, C., Meyers, S.R., Lourens, L.J., Hilgen, F.J., 2015. Testing astronomically tuned age models. Paleoceanography 30, 369–383. https://doi.org/10.1002/2014PA002762.

Zeeden, C., Meyers, S.R., Hilgen, F.J., Lourens, L.J., Laskar, J., 2019. Time scale evaluation and the quantification of obliquity forcing. Quat. Sci. Rev. 209, 100–113. https://doi.org/10.1016/j.quascirev.2019.01.018.